Modelling and Dynamic Response of a Damper with Relief Valve

R.D. Eyres *, A.R. Champneys, N.A.J. Lieven

Bristol Laboratory for Advanced Dynamic Engineering, University of Bristol, Queens Building, University Walk, Bristol, BS8 1TR, U.K.

Abstract

This paper outlines several possible method of modelling a passive hydraulic damper with a bypass tube that is opened by a precompressed relief valve. Initially a simple algebraic model is derived which is developed into a more computationally complex model incorporating the dynamics of the internal spring valve and fluid compressibility. Numerical simulations indicate realistic dynamical phenomena and suggest key design parameters.

Key words: Hydraulic damper, relief valve, fluid compressibility
PACS:

Content:
43 pages of text; 1 table; 19 figures

1 Introduction

Vibration dampers are used in many applications such as car shock absorbers [1], bridge stabilisation [2], helicopters [3][4][5] and earthquake-resistant buildings [6][7]. A model is essential if changes are to be investigated without reconstructing the system. This paper will concentrate on a damper as a stand alone module within a larger mechanical system. Hence it is assumed that a simple, time dependent input displacement produces a force. The damper modelled is essentially a plunger in hydraulic fluid. The plunger has a small orifice that connects either side through which the fluid flows, as in figure 1. There is an added complication on the damper studied. When the pressure

* Corresponding author. Tel.: +44-117-928-9860; fax: +44-117-927-2771.
Email address: richard.eyres@bristol.ac.uk (R.D. Eyres).

difference between the two sides of the plunger is high enough, a conical valve opens that allows fluid to flow through an alternative tube as in figure 2. When this occurs the damper is said to *'blow-off'* . The blow-off valve is connected to the damper's casing via a spring. The precompression of the spring against the alternative *'bypass tube'* determines the pressure difference at which the valve will open. The blow-off system is the same for negative pressure differences with the valve resting against a second bypass tube preventing fluid flowing freely in the opposite direction. Such a damper is indicative of that used in applications where the damping of small amplitude or low frequency motion is most important.

This study has been motivated by the attempt to reproduce some propriotory test data that shows a hydraulic damper configured as in figures 1 and 2. The broad features of this data are: hysteresis; delayed response; and chattering oscillations in the blow-off region. Figure 3 is a qualitative sketch of a typical input to the system. The plot shows the damper piston's displacement against time. The main feature of the sketch is the smoothness of the periodic motion and the small number of changes in the displacement gradient. From this type of input we require a force qualitatively similar to that shown in figure 4. The force against time sketch shows local rapid oscillations at high forces. The direction of the force does not change in these regions as might be expected from the displacement gradients suggesting some kind of delayed response in the output. The hysteresis is more evident in the force against velocity sketch. The hysteresis results in a minimal response to high frequency changes in input displacement while allowing a smoother response to the larger low frequency components.

A dynamic fully parametric model of such a damper is pressing due to the interations between the spring compression and overall pressure in the tube. As shown later this can lead to a complex dynamic response. While semi-empirical models of dampers such as in figure 1 have received attention [8][9][10][11], to our knowledge the effects of the passive blow-off valve have not been treated in the literature (although relief valves treated on their own have been shown to lead to nonlinear [12][13] and chaotic dynamics [14].) The resulting model can be used to predict the effect of changing the properties of the damper on the dynamic response. The key features investigated are the sizes of the orifice and bypass tube along with the stiffness and discharge characteristics of the spring and valve respectively. In this paper a simple lumped mass parametric model is derived that incorporates all these effects.

The rest of this paper is outlined as follows. Section 2 describes the modelling process used by previous researchers to model figure 1 as a simplification of an automobile shock absorber. Sections 3 and 4 investigate several possible extensions to the model in section 2 to take into account the blow-off. First an explicit model is derived to give the force for a given displacement input.

The relief valve and compressibility of the fluid are then considered separately. A model for the whole system is then derived. Section 5 gives some results using the different models using indicitive parameter values. There is also a discussion in section 6 on a possible optimisation technique to optimise the energy dissipation. Finally section 7 discusses the relative merits of each of the models.

2 Hydraulic dampers

The two most common types of dampers in widespread use as vibration absorbers are: passive dampers; and semi-active dampers. Passive dampers such as hydraulic dampers or elastomeric dampers require no external input to operate and perform in a totally passive way. Active dampers have an external energy input so that the force response from a given input can be changed to suit the conditions. This can lead to high energy requirements which is why semi-active dampers are now becoming more popular. Semi-active dampers are similar to active dampers but they have input forces that are orders of magnitude smaller than for active dampers. An analogy can be made with the fluid orifice damper in figure 1. A passive damper's response would remain the same for all time (ignoring wear etc.) whereas a possible semi-active damper would be able to mechanically change the size of the main orifice so producing a different response characteristic. To fully understand this type of semi-active damper it is important to understand the simple passive case so that control laws can be derived.

It is essential that a parametric model is derived rather than modelling the dampers simply by their characteristics with transfer functions. While the transfer function method can produce a simpler and quicker solution, it can not take into account the physics of the system. Changing the orifice diameter for example would require the damper to be rebuilt and the model fitted again to the new test data. This would not be required if a parametric model was implemented, except for verification.

The passive damper used in many applications is essentially similar to that of an automobile shock absorber. Work on modelling such systems has been performed by a number of groups. The resulting equations are all based around the same basic equation taken from work by Wallaschek [1] and later developed by Worden, Tomlinson, Surace and co-workers [8][9][10][11] based upon a thesis by Lang [15] in 1977. Referring to figure 1, an equation for the force provided by the damper is defined as

$$
\begin{aligned}
& F(t) = m\ddot{y}(t) + A[P_1(t) - P_2(t)] + f_c \text{sign}(\dot{y}(t)), \\
\text{where} \quad & P_i(t) = \text{Pressure in chamber } i.
\end{aligned} \tag{1}
$$

The equation states that the force on the piston caused by a given motion $y(t)$ applied to the damper is given as the sum of the inertia of the body $m\ddot{y}(t)$, the force on the piston due to the difference in pressure between the two chambers $A[P_1(t) - P_2(t)]$ and the friction due to the piston rubbing against the sides which is assumed to be a constant force f_c. Here A is the cross-sectional area of the chamber.

The pressure difference $[P_1(t) - P_2(t)]$ can be attributed to the sum of viscous frictional losses through the orifice Δp_f and head loss at the exit of the orifice Δp_h.

Assuming incompressibility, the continuity equation can be used to obtain the change in volume in the chamber, $\dot{V}$,

$$
\dot{V} = A\dot{y}. \tag{2}
$$

For small $\dot{y}$ the flow can be assumed to be laminar. Poisseuille's equation [16] can then be used to express $\dot{V}$ in terms of the pressure difference Δp_f between the two chambers due to viscous losses:

$$
\dot{V} \quad = \quad \frac{\pi d^4 \Delta p_f}{128 l \eta}, \tag{3}
$$

where η is the dynamic viscosity, l is the length of the orifice and d is its diameter (assumed circular in cross-section).

Combining (2) and (3) yields the following equation for the viscous forces through the orifice,

$$
\Delta p_f \quad = \quad 8 l \eta \pi \left(\frac{A}{A_o^2} \right) \dot{y}(t), \tag{4}
$$

where A_o is the area of the orifice.

The second contribution to pressure loss Δp_h is due to the head loss (sometimes called *throttle loss*) at the exit of the orifice given by

$$
h_L = c \frac{v_o^2}{2g}, \tag{5}
$$

where v_o is the velocity of the flow through the constriction. For a sharp 90^o exit, c has a value of 0.5 [17]. Conservation of momentum states that $\dot{y}A = v_o A_o$. Hence

$$h_L = c\left(\frac{A}{A_o}\right)^2 \frac{1}{2g}\dot{y}^2(t),$$

and so

$$\Delta p_h = h_L \rho g = \frac{1}{2}c\rho\left(\frac{A}{A_o}\right)^2 \dot{y}^2(t)\text{sign}(\dot{y}(t)), \tag{6}$$

where ρ is the density of the fluid. The difference in pressure $P_1 - P_2$ is equal to the loss described in (4) and (6),

$$[P_1(t) - P_2(t)] = \Delta p_f + \Delta p_h.$$

The overall equation of motion is therefore given by

$$F(t) = m\ddot{y}(t) + d_1\dot{y}(t) + d_2\dot{y}^2(t)\text{sign}(\dot{y}(t)) + d_3\text{sign}(\dot{y}(t)), \tag{7}$$

where

$$d_1 = 8l\eta\pi\left(\frac{A}{A_o}\right)^2,$$
$$d_2 = \frac{1}{2}c\rho\left(\frac{A}{A_o}\right)^2 A,$$
$$d_3 = f_c.$$

With a purely sinusoidal input, $y(t) = Y\sin\omega t$, an algebraic equation is produced as given by Surace et al [9]:

$$F(t) = -mY\omega^2\sin(\omega t) + d_1 Y\omega\cos(\omega t) + d_2 Y^2\omega^2\cos^2(\omega t)\text{sign}(\cos\omega t) + d_3\text{sign}(\cos\omega t). \tag{8}$$

In [9] this equation was solved using an Euler scheme. There were problems with this approach as with any numerical scheme applied to a model with Heaviside nonlinearities. There is therefore a need to develop an explicit method of simulating the system along with time-step approaches as shown in section 4.

3 Incorporating the blow-off dynamics

The model can be extended to incorporate more realistic dynamics that result from the relief valve and blow-off region. As stated in the introduction, the damper to be studied has a blow-off region where the fluid is allowed to recirculate through a bypass valve rather than having to flow through the main orifice in the piston. See figure 2. The valve will open when a pre-set force (F_{crit}) is exerted upon it by the flow through the recirculation pipe ($F > F_{crit}$). This recirculation acts as an alternative orifice. In the simplest possible model we can treat the damper with the bypass tube open in exactly the same way as the original orifice but with a different geometry. The area of the orifice now becomes the area of the bypass tube A_b rather than A_o since $A_o << A_b$. Hence we use (7) with different coefficients consequent on the motion now having four different regions:

i low force ($F < F_{crit}$), damper in compression ($\dot{y} > 0$);
ii high force ($F > F_{crit}$), damper in compression ($\dot{y} > 0$);
iii low force ($F < F_{crit}$), damper in rebound ($\dot{y} < 0$); and
iv high force ($F > F_{crit}$), damper in rebound ($\dot{y} < 0$).

Four seperate possibilities are considered in the next two sections. These are: more careful treatment of the critical force F_{crit}; backlash in section 4.1; change in flow due to the spring valve in section 4.2; and compressibility in section 4.3. In section 4.4 these are pulled together into a single comprehensive model.

In this section the system is considered as a set of explicit formulae rather than using a timestepping technique. The aim is to predict F for a given input displacement $y = Y\sin(\omega t)$.

3.1 Constant pressure model

From section 2 it is not clear what the value of d_3 should be when the valve is open. The value can be calculated in the simplest case using (8) if the critical force is known to be exceeded through the motion. However the input to the damper will not always be so simple. Physical reasoning needs to be applied if the parameters are to be chosen correctly. This section outlines a simplifying assumption that can be made to model the transition from low force ($F > F_{crit}$) when the valve is closed, to high ($F < F_{crit}$) force when the relief valve is open. A physical explanation for the motion in the blow-off region will be discussed. The overall equation of motion, ignoring the transition region, is given in (9).

$$F(t) = \begin{cases} m\ddot{y}(t) + d_1^{(1)}\dot{y}(t) + d_2^{(1)}\dot{y}^2(t)\text{sign}(\dot{y}(t)) + d_3^{(1)}\text{sign}(\dot{y}(t)) \text{ if } |F| < F_{crit} \\ m\ddot{y}(t) + d_1^{(2)}\dot{y}(t) + d_2^{(2)}\dot{y}^2(t)\text{sign}(\dot{y}(t)) + d_3^{(2)}\text{sign}(\dot{y}(t)) \text{ if } |F| > F_{crit} \end{cases} \tag{9}$$

The only unknown parameter in (9) is $d_3^{(2)}$. It is calculated to give equivalent results to those observed. Problems may arise if the selection is incorrect since the fitting of physical parameters to each coefficient $d_i^{(j)}$ is nontrivial.

The size of the main chambers (chamber 1 and chamber 2 in figures 1 and 2) can be assumed to be large compared to the size of the orifice and bypass tube. An analogous model can be thought of as a barrier separating chambers 1 and 2 with three holes in, the larger blocked with the spring loaded valves (one for each direction of flow) as in figure 5.

At lower pressures all the flow will pass through the piston orifice as the valve will remain closed due to the spring precompression. This will be the case up to the critical force F_{crit}. Above this force as the flow rate increases, a valve will open allowing some of the fluid to flow through the bypass tube. If chamber 1 can be thought of as having a large volume, the change in pressure in chamber 1 due to the additional fluid flowing through the bypass tube will be negligible. This means that the pressure differential across the piston orifice will remain approximately constant for all forces greater than the critical force, so the orifice flow will remain constant. This implies that the contribution to the force due to the piston orifice remains the same and equal to the critical force F_{crit}. The extra flow through the bypass tube will cause an additional force which can be added to F_{crit}.

The overall equation now becomes, referring to figure 6,

$$F(t) = \begin{cases} m\ddot{y}(t) + d_1^{(1)}\dot{y}(t) + d_2^{(1)}\dot{y}^2(t)\text{sign}(\dot{y}(t)) + d_3^{(1)}\text{sign}(\dot{y}(t)) \text{ if } |F| < F_{crit} \\ F_{crit} + m\ddot{y}(t) + d_1^{(2)}\left(\dot{y}(t) - \dot{y}_{crit}\right) \text{ if } |F| > F_{crit}, \end{cases} \tag{10}$$

where

$$
\begin{aligned}
d_1^{(1)} &= 8l\eta\pi \left(\frac{A}{A_o}\right)^2, \\
d_2^{(1)} &= \frac{1}{2}c\rho \left(\frac{A}{A_o}\right)^2 A, \\
d_3^{(1)} &= f_c, \\
d_1^{(2)} &= 8l_b\eta\pi \left(\frac{A}{A_b}\right)^2, \\
t_0 &= \text{calculated time of critical force}, \\
l_b &= \text{length of bypass tube}, \\
A_b &= \text{cross-sectional area of bypass tube},
\end{aligned}
$$

if it is assumed that the bypass orifice is large enough to avoid head losses at the exit. Computationally this may cause a problem as $\dot{y}_{crit}$ will need to be calculated for each blow-off. Alternatively, an exact value for the non-physical $d_3^{(2)}$ in (9) (see figure 6) can be calculated as the critical force and time is known for the first intersection. The equation to calculate $d_3^{(2)}$ for a sinusoidal input will be

$$d_3^{(2)} = F_{crit} + mYw^2 \sin(wt_{crit}) - d_1^{(2)} wY \cos(wt_{crit}),$$

where t_{crit} is calculated at the intersection of the low force trajectory and the critical force at $\dot{y}_{crit}$.

3.2 **Equivalent velocity model**

It would be simpler to analyse the system if the whole cycle for a given input displacement could be described by the flow through the main orifice. This section is an extension to section 3.1 and aims to calculate this *effective flow* through the orifice assuming a smooth transition and taking into account the blow-off region.

Ignoring compressibility, the flow due to the motion of the piston will be completely shared in some proportion between flow through the orifice (Q_o) and flow via the bypass tube (Q_b). This can be expressed as

$$Q_o + Q_b = A\dot{y}. \tag{11}$$

The head loss due to the two flows (and so the corresponding pressure difference) must be equal as discussed in [18] with applications to pipe networks. As a simple example, this implies that a wider pipe would need more flow through it to produce the same head loss as a similar but narrower pipe. The

loss coefficients would define the ratio of flow rate. The idea can be applied to (9) with reference to figure 6.

The case shown in figure 6 takes a velocity of $\dot{y}_1$ giving a pressure difference P_1. For the head loss to be the same for both routes (orifice and bypass), and hence the pressure difference, the *equivalent velocity* for the main orifice would be given by $\dot{y}_e$. This is calculated using the equation for the main orifice ($F < F_{crit}$) from (9), ignoring the inertia and friction of the piston. The flow through the bypass tube will therefore given by

$$Q_b = A(\dot{y}(t) - \dot{y}_e(t)).$$

There are now two equations for the pressure P_1 or force

$$\begin{aligned} P_1 A &= d_1^{(1)}\dot{y}_e(t) + d_2^{(1)}\dot{y}_e(t)^2\text{sign}(\dot{y}_e(t)), \\ P_1 A &= d_1^{(2)}\dot{y}(t) + d_2^{(2)}\dot{y}(t)^2\text{sign}(\dot{y}(t)) + d_3^{(2)}\text{sign}(\dot{y}(t)), \end{aligned}$$

which can be equated and solved to give an equation for the effective velocity through the orifice for a given piston velocity, $\dot{y}(t)$, above the critical velocity, $\dot{y}_{crit}$, as

$$\dot{y}_e(t) = \frac{-d_1^{(1)} + \sqrt{\left(d_1^{(1)}\right)^2 + 4d_2^{(1)}\left[d_1^{(2)} + d_2^{(2)}\dot{y}(t)|\dot{y}(t)| + d_3^{(2)}\text{sign}(\dot{y}(t))\right]\text{sign}(\dot{y}(t))}}{2d_2^{(1)}\text{sign}(\dot{y}(t))},$$

since $\text{sign}(\dot{y}(t)) = \text{sign}(\dot{y}_e(t))$. The system can now be fully described by the flow through the orifice.

4 Modelling further effects

4.1 Backlash

An additional backlash term can also be incorporated into the main damper system [1] due to loose connections of the damper. A suggested model is given in (12), where $\hat{y}$ is the amplitude of oscillation.

$$F(t) = m\ddot{y} \text{ if } \begin{cases} y(t) - \hat{y} < \delta \quad \text{and} \quad \dot{y} < 0, \text{ or} \\ y(t) + \hat{y} < \delta \quad \text{and} \quad \dot{y} > 0 \end{cases}$$
$$F(t) = m\ddot{y}(t) + d_1\dot{y}(t) + d_2\dot{y}^2(t)\text{sign}(\dot{y}(t)) + d_3\text{sign}(\dot{y}(t)), \text{ otherwise.} \quad (12)$$

A second point of note is the negligible contribution from the Coulomb friction term f_c in (1). There is no indication of Coulomb friction in the available test data. The backlash may hide this so further experimentation needs to be carried out. The rest of this paper will assume there is no contribution from backlash or Coulomb friction. Hence $d_3^{(1)} = 0$ in what follows.

4.2 Change in flow due to relief valve

Section 3.2 can be extended to include the dynamics of the spring-loaded relief valve. There are three parts in the system that can produce a pressure differential (again ignoring compressibility):

(a) flow through piston orifice;
(b) flow through bypass tube; and
(c) flow past the valve.

The pressure difference between the two chambers must be the same as discussed in section 3.2. The pressure loss due to the orifice must therefore be the same as the loss due to the bypass tube and valve combined, so

$$\Delta P = \Delta P_b + \Delta P_v, \quad (13)$$

where ΔP_v is the pressure loss due to flow past the valve and ΔP_b is the pressure loss due to flow through the bypass tube. Hayashi et al [14] used (14) to define the flow, Q_v, past a simple valve similar to the one in figure 2 with a pressure loss ΔP_v and a valve displacement X from the valve seat.

$$Q_v = C_{po}\left(\frac{\gamma X}{1+\gamma X}\right) X\pi d_v \sin(\alpha)\sqrt{\frac{2\Delta P_v}{\rho}}, \quad (14)$$

C_{po} and γ are experimentally determined, d_v is the diameter of the valve and α is the half angle of the valve. The pressure difference due to flow through the main orifice can be adapted from (7) to give the pressure loss in terms of flow rates

$$\Delta P = D_1 Q_o + D_2 Q_o |Q_o|, \tag{15}$$

where

$$D_1 = \frac{128 l \eta}{\pi d^4}, \tag{16}$$

from (3) and

$$D_2 = \frac{c\rho}{2A_o^2}, \tag{17}$$

from (5). Similarly for the pressure loss due to the flow through the bypass tube

$$\Delta P_b = B_1 Q_v + B_2 Q_v |Q_v|, \tag{18}$$

where B_1, B_2 are as D_1, D_2 with the bypass tube dimensions, and $Q_b = Q_v$ in the incompressible case.

Using (11), (13), (14), (15) and (18) with the substitution

$$R(X) = C_{po}\left(\frac{\gamma X}{1+\gamma X}\right) X \pi d_v \sin(\alpha)\sqrt{\frac{2}{\rho}}$$

yields

$$Q_v = R(X)\sqrt{D_1(A\dot{y} - Q_v) + D_2(A\dot{y} - Q_v)|A\dot{y} - Q_v| - B_1 Q_v - B_2 Q_v |Q_v|},$$

so

$$\begin{aligned} Q_v = \Big[& -R(X)^2(D_1 + 2D_2 A_p \dot{y} + B_1) \\ & \pm \sqrt{[R(X)^2(D_1 + 2D_2 A_p \dot{y} + B_1)]^2 + 4(1 - R(X)^2(D_2 - B_2))(R(X)^2(D_1 A_p \dot{y} + D_2(A_p \dot{y})^2))} \Big] \\ & \Big/ 2(1 - R(X)^2(D_2 - B_2)). \end{aligned} \tag{19}$$

The solution to this, Q_v, substituted back into (14) produces the overall equation for the pressure difference across the valve as a function of piston velocity and valve displacement given by

$$\Delta P_v = \left(\frac{Q_v}{R(X)} \right)^2,$$

so then

$$\begin{aligned} \Delta P_v = \Bigg[\Bigg(& -R(X)(D_1 + 2A\dot{y}D_2 + B_1) \\ & + \sqrt{R(X)^2(D_1 + 2A\dot{y}D_2 + B_1)^2 + 4(1 - R(X)^2(D_2 - B_2))(D_1 A\dot{y} + D_2(A\dot{y})^2)} \Bigg) \\ & \Big/ 2\left[1 - R(X)^2(D_2 - B_2)\right] \Bigg]^2. \end{aligned} \tag{20}$$

The force on the valve F_v, cross sectional area A_v, will be

$$F_v = A_v \Delta P_v, \tag{21}$$

which can be substituted into the equation of motion for the valve (22)

$$m_v \ddot{X} + \delta \dot{X} + k(X + X_c) = F_v, \tag{22}$$

with the condition

$$(X, \dot{X}) = \begin{cases} (X, \dot{X}) & \text{if } X > 0, \\ (0, 0) & \text{otherwise,} \end{cases}$$

where m_v is the effective mass of the valve and spring, δ is the damping constant, k is the linear spring stiffness and X_c is the precompressed offset of the spring. The solution, $X(t)$, to the differential equation is put into (19) to yield Q_v and hence Q_o from (11). The force on the piston is then given by (15) multiplied by A_p as in (1) without Coulomb friction or inertia.

4.3 **Compressibility**

An extension to the basic model seen in (1) would be to include the effect of the compressibility of the hydraulic fluid. Lang [15] also included the expansion of the damper casing as a contributing factor, however this will not be considered. The analysis below mirrors closely that of Worden and Tomlinson [8][9][10].

From conservation of mass (m) [17], where V is the volume of fluid,

$$m = \rho V,$$

so differentiation gives

$$dm = \rho dV + V d\rho,$$

and as $dm = 0$ we get

$$\rho dV = -V d\rho.$$

Let's assume $\rho(p)$ and $V(p)$ so therefore

$$\frac{1}{\rho}\frac{d\rho}{dp} = -\frac{1}{V}\frac{dV}{dp}.$$

From this the compressibility of the fluid is defined to be

$$\beta = -\frac{1}{V}\frac{dV}{dp}.$$

Rearranging using the chain rule gives

$$\frac{dV}{dt} = -\beta V \frac{dp}{dt}. \tag{23}$$

The rate of change of volume in chamber i is the difference between the volume rate displaced by the piston's motion ($A_i\dot{y}$) and the actual volume rate of fluid moving from one chamber to the other ($\dot{V}$). If this value is zero then this suggests the fluid has not been compressed. Equation (23) can be used with this to give the rate of change of pressure in each chamber as

$$\frac{dp_1}{dt} = \frac{A_1\dot{y}(t) - \dot{V}(t)}{\beta V_1(t)}, \tag{24a}$$

$$\frac{dp_2}{dt} = -\frac{A_2\dot{y}(t) - \dot{V}(t)}{\beta V_2(t)}. \tag{24b}$$

Two assumptions can now be made to make the formulation of an overall equation easier to find. Firstly, let $A_1 = A_2 = A$ as with all previous analysis (i.e. a symmetric piston). Secondly we can assume that the volume of the fluid in each chamber, V_i, is large in comparison its change in volume (relatively small damping stroke). If this is the case then $V_1(t) = \zeta V_2(t) = \overline{V}$ where $\overline{V}$ is the average volume of chamber 1 and ζ is some constant to take into account the different sizes of chambers. This is different from previous studies. Equation (24) can then be simplified to show

$$\frac{dp_1}{dt} = -\frac{1}{\zeta}\frac{dp_2}{dt},$$

so

$$\zeta\frac{dp_1}{dt} + \frac{dp_2}{dt} = 0,$$

giving

$$\zeta p_1 + p_2 = constant, \tag{25}$$

so a convenient choice of variable to describe both pressures is

$$p_1 - p_2 = z, \tag{26}$$

where z is the thermodynamic variable [10]. If z is known, p_i can be calculated using (25) and (26). Using this and (24) gives

$$\dot{z}(t) = \frac{dp_1}{dt} - \frac{dp_2}{dt} = \frac{1+\zeta}{\zeta\beta\overline{V}}\left(A\dot{y}(t) - \dot{V}(t)\right) \tag{27}$$

Equation (7) states that that the difference in pressure between the two chamber can be attributed to the viscous losses through the orifice and the head loss at the entrance to the orifice as in section 4.2. For compressible flow the

pressure difference needs to be in terms of volume flow rates to give a quadratic expression in terms of $\dot{V}(t)$:

$$z(t) = D_1\dot{V}(t) + D_2\dot{V}(t)^2\text{sign}(\dot{V}(t)), \tag{28}$$

where D_1 and D_2 are as (16) and (17) respectively. This can be solved yielding

$$\dot{V}(t) = \frac{-D_1 \pm \sqrt{D_1^2 + 4D_2 z(t)\text{sign}(\dot{V}(t))}}{2D_2\text{sign}(\dot{V}(t))}. \tag{29}$$

It can be assumed that $\text{sign}(\dot{V}) = \text{sign}(z)$ since there cannot be flow in the opposite direction to the pressure gradient for a uniform pipe. From this assumption

$$\begin{aligned} &\text{sign}(\dot{V})z = \text{sign}(\dot{V})|z|\text{sign}(z), \text{ so} \\ &\text{sign}(\dot{V})z = +|z|. \end{aligned} \tag{30}$$

(29) and (30) combine to produce

$$\dot{V}(t) = \text{sign}(z(t))\left[\frac{-D_1 \pm \sqrt{D_1^2 + 4D_2|z(t)|}}{2D_2}\right]. \tag{31}$$

(31) can be simplified for the two cases $z < 0$ and $z > 0$.

case *(i)* $z < 0$

Equation (31) becomes

$$\dot{V}(t) = \frac{D_1 \mp \sqrt{D_1^2 + 4D_2|z(t)|}}{2D_2}.$$

Since $D_1 > 0$ and $D_2 > 0$,

$$2D_2\dot{V} = D_1 - \sqrt{D_1^2 + 4D_2|z(t)|} \quad < 0 \tag{32a}$$

$$2D_2\dot{V} = D_1 + \sqrt{D_1^2 + 4D_2|z(t)|} \quad > 0 \tag{32b}$$

and $\dot{V} < 0$, only (32a) can be true.

case *(ii)* $z > 0$

In a similar way to case i ,

$$2D_2\dot{V} = -D_1 + \sqrt{D_1^2 + 4D_2|z(t)|} \quad > 0 \tag{33a}$$

$$2D_2\dot{V} = -D_1 - \sqrt{D_1^2 + 4D_2|z(t)|} \quad < 0 \tag{33b}$$

so only (33a) can be true.

The two cases can be combined with (27) to give

$$\dot{z}(t) = \frac{1+\zeta}{\zeta\beta\overline{V}}A\dot{y}(t) + \text{sign}(z)\frac{1+\zeta}{\zeta\beta\overline{V}}\left(\frac{D_1 - \sqrt{D_1^2 + 4D_2|z(t)|}}{2D_2}\right) \tag{34}$$

The solution of the equations are then put into

$$m\ddot{y} + Az = F \tag{35}$$

to give the overall force produced by the damper.

4.4 **Overall dimensionless model**

It is now possible to combine sections 4.2 and 4.3 to give an overall set of equations for the damper system.

The motion of the valve will have the same general form as in section 4.2 (22). A simplification can be made to allow a simply coupled equation between the valve motion and the compressibility of the fluid. Section 3.1 argued that the losses through the bypass tube are essentially linear due to the relatively large diameter of the bypass tube compared to the main orifice. This argument can be taken one step further. The linear losses in the bypass tube can be assumed to be negligible compared to the losses due to flow through the main orifice and the losses due to flow past the relief valve from section 4.2. Using this simplification, the pressure loss due to the orifice must be the same as the pressure loss due to the relief valve alone. The force on the valve is therefore from the difference in pressure between the two chambers rather than having to incorporate the difference in pressure due to the bypass tube. The equation of motion for the valve becomes

$$m_v\ddot{X} + \delta\dot{X} + k(X + X_c) = A_v z,$$

where z is the pressure difference between the chambers as in section 4.3.

The compressibility equation (27) can be modified to include the flow past the relief valve when the valve is open. The rate of change in volume of a chamber is still the difference in volume displaced by the piston ($A\dot{y}$) and the actual volume flowing between chambers. Now the volume flowing between chambers is the sum of the flow through the orifice and the flow through the bypass tube ($\dot{V} + Q_v$). The additional compressibility effects within the bypass tube can be ignored as the volume in the tube is small compared to the volume of the chambers. The general compressibility equation now becomes

$$\dot{z}(t) = \frac{1+\zeta}{\zeta\beta\overline{\overline{V}}}\left(A\dot{y}(t) - \dot{V}(t) - Q_v(t)\right).$$

The expression for $\dot{V}$ will be the same as before

$$\dot{V} = \text{sign}(z)\left(\frac{-D_1 + \sqrt{D_1^2 + 4D_2|z(t)|}}{2D_2}\right),$$

and the equation for flow past a valve will remain the same (14) with $\Delta P_v = z$.

The system can now be summarised as a set of three differential equations where F_{crit} is the force at which the valve opens. For the purposes of this paper it has been assumed that the damper system is symmetric for compression and rebound. This means the valve properties such as their stiffness, k, precompression, X_c, and dimensions are the same for both valves. This simplification results in a reduction in the number of equations required. The damper can be thought of as having just one valve since the case of both valves being open at the same time is not observed in practice since the forcing frequencies are too low. The valve will act as a bypass route for both compressive and rebound strokes.

case *(i)* $A_v z > F_{crit}$ (valve open)

$$\begin{cases} \ddot{y}(t) &= (F(t) - Az(t))/m, \\ \ddot{X}(t) &= (A_v z(t) - \delta\dot{X}(t) - k(X(t) + X_c))/m_v, \\ \dot{z}(t) &= \frac{1+\zeta}{\zeta\beta\overline{\overline{V}}}\left[A\dot{y}(t) - \text{sign}(z(t))\left(\frac{-D_1+\sqrt{D_1^2+4D_2|z(t)|}}{2D_2}\right) - \text{sign}(z(t))R(X,t)\sqrt{|z(t)|}\right], \end{cases} \tag{36}$$

where

$$R(X,t) = C_{po}\left(\frac{\gamma X(t)}{1+\gamma X(t)}\right) X(t)\pi d_v \sin(\alpha)\sqrt{\frac{2}{\rho}}.$$

case *(ii)* $A_v z < F_{crit}$ (valve closed)

$$\begin{cases} \ddot{y}(t) & = (F(t) - Az(t))/m, \\ \ddot{X}(t) & = 0, (\dot{X}(t), X(t)) = (0,0), \\ \dot{z}(t) & = \frac{1+\zeta}{\zeta\beta\overline{V}}\left[A\dot{y}(t) - \text{sign}(z(t))\left(\frac{-D_1+\sqrt{D_1^2+4D_2|z(t)|}}{2D_2}\right)\right]. \end{cases} \tag{37}$$

The system can be nondimensionalised using

$$\begin{aligned} t &= T\tau \\ F(t) &= fG(\tau) \\ z(t) &= \xi Z(\tau) \\ y(t) &= \nu Y(\tau) \\ X(t) &= hH(\tau) \end{aligned}$$

where τ, G, Z, Y, H are nondimensionalised time, force, pressure, piston displacement and spring deflection respectively and $'$ is the derivative with respect to τ. An assumption has been made that the contribution to the overall force due to the inertia of the piston is minimal. The maximum acceleration achieved in a cycle is of the order of 25 m/s^2 which is several orders of magnitude less than the force generated by the damper. An illustration of this can be seen in figure 7. The two cases of no inertia and a large piston mass of 10kg are almost identical with the maximum difference between the two cases of 0.8%. The negligable contribution of the piston inertia means the first force equation in (36) and (37) becomes

$$F(t) = Az(t). \tag{38}$$

The resulting nondimensionalised system can now be expressed as

case *(i)* $Z > Z_{crit}$ (valve open)

$$\begin{cases} G(\tau) & = Z(\tau), \\ H''(\tau) & = Z(\tau) - c_1 H'(\tau) - c_2 H(\tau) + c_3, \\ Z'(\tau) & = Y'(\tau) - \text{sign}(Z(\tau)) \left[-1 + \sqrt{1 + |Z(\tau)|} + c_4 \left(\frac{H(\tau)^2}{1 + c_5 H(\tau)} \right) \sqrt{|Z(\tau)|} \right] \end{cases} \tag{39}$$

case *(ii)* $Z < Z_{crit}$ (valve closed)

$$\begin{cases} G(\tau) & = Z(\tau), \\ H''(\tau) & = 0, (H'(\tau), H(\tau)) = (0, 0), \\ Z'(\tau) & = Y'(\tau) - \text{sign}(Z(\tau)) \left[-1 + \sqrt{1 + |Z(\tau)|} \right]. \end{cases} \tag{40}$$

The corresponding dimensionless parameters are given by

$$\begin{aligned} T &= \frac{D_1 \beta \overline{V}}{4}, & f &= \frac{A D_1^2}{4 D_2}, & \xi &= \frac{D_1^2}{4 D_2}, \\ \nu &= \frac{D_1^2 \beta \overline{V}}{8 D_2 A}, & h &= \frac{A_v D_1^4 (\beta \overline{V})^2}{64 D_2 m_v}, & c_1 &= \frac{\delta T}{m_v}, \\ c_2 &= \frac{k T^2}{m_v}, & c_3 &= \frac{k T^2 X_c}{m_v h}, & c_4 &= \frac{2 T C_{po} \gamma h^2 \pi d_v \sin(\alpha) \sqrt{2\xi}}{\xi \beta \overline{V} \sqrt{\rho}}, \\ c_5 &= \gamma h. \end{aligned}$$

The values taken for these parameters are given in table 1. T is the nondimensionalising parameter for time, f for the force generated by the damper, ξ for the pressure diference, ν for input displacement and h for spring displacement. The other parameters are nondimensional combinations of the original physical constants. We can change these physical constants and directly link the change to the new dimensionless parameters. For example key properties for the damper will be the compressibility β and orifice diameter d. Changes in these values will not necessarily lead to an obvious change in the equations as before. Doubling the value of β will double T and ν, increase h by a factor of 4 and halve c_4. Any changes in the dimensionless parameters have to be linked back to the physical properties if any information is to be gained from the results.

5 Dynamic response

The proposed models can be qualitatively compared to each other. They can also be uesd to investigate changes in the parameters which are directly linked to the physical properties of the damper. For example a change in the viscosity of the hydraulic fluid will linearly change d_1 in (7). We will look at each modelling technique in turn and present results for each.

5.1 Explicit model

In the first part of this section two simplifications will be made on the algebraic model (8) so that the fundamental dynamics of the system can be investigated. The first assumption is that the displacement input is sinusoidal with equation $y(t) = \sin(t)$, so $Y = \omega = 1$. The second simplification is that the inertia of the piston is negligable compared to the maximum force produced by the damper so set $m = 0$ in (7) and (8). The value of $d_3^{(2)}$ is calculated using a Newton-Raphson scheme and substituted into the system equation to give a smooth transition from low to high force. Figure 8 gives an idea of the effects of parameter changes on the force-velocity profile.

The reference plot in figure 8 is the solid line with the parameter values listed. It has a quadratic profile with a blow-off force of 0.5N. Many dampers are design to be *linear* devices (i.e. $F(t) = C\dot{y}(t)$). This is achieved by changing the way the fluid passes through the piston. Many examples of this are used in civil engineering structures to combat earthquake vibrations in tall buildings [19]. A similar damper can be modelled by setting $d_2^{(1)}$ to zero as in figure 8, shown by the dotted line. The force against velocity graph is now linear for both regions (high and low forces).

The effect of changing the critical force can be seen as the $-+-$ line. This is achieved by adjusting the relief valve so that it opens at a lower force (decrease X_c as discussed in section 4.2). If this is the only parameter that has changed, the system will be in the blow-off region for longer. The maximum force will be less, hence less energy dissipated for a given sinusoidal input.

As suggested in the introduction to section 5 a change in $d_1^{(1)}$ will change the response as shown on the $-\diamond-$ line. The linear part of the low force equation has doubled so the force reaches the critical value at a lower velocity. This implies a greater energy dissipation as discussed in section 6.

When incorporating the extensions to the algebraic model, the general large-scale dynamics of the system will remain the same. The only difference between the model discussed in section 2 and the models in section 3 is the transition

region from high to low force. There is however no significant change in the overall dynamics. The current algebraic model can be qualitatively compared with the later models using the same input displacement curve given in (41) as plotted in figure 9. The input was chosen as it displays both high and low frequency characteristics as in figure 3 which is typical of many applications.

$$y(t) = 2.5\cos(30t) + 4\sin(30t) + 0.25\cos(60t) + 5\sin(60t) + 0.9\cos(90t) - 0.3\sin(90t) + 0.4\cos(120t) + 0.2\sin(120t) + 0.05\cos(150t) - 0.3\sin(150t). \tag{41}$$

Using the displacement in (41) the simple algebraic model (7) can be applied. The resulting force can be seen in figure 10. It is clear that the model does not sufficiently capture the required dynamics. The system is too responsive to high frequency changes in velocity in the force vs time plot compared to the observations summarised in figure 4. Furthermore the results do not show any hysteresis in the force vs velocity plot.

5.2 **Time-stepping approach**

Since the simple algebraic model does not display the required characteristics, there is no need to investigate the effects of the extensions to the model in section 3. Instead focus turn to the more accurate differential equation model derived in sections 4.2, 4.3 and 4.4, which were solved using MATLAB ODE45 [20].

The aim of the time-stepping approach was to produce a more realistic model of the damper system incorporating the spring valve and compressibility. This section is therefore aimed at trying to find the set of parameters that best describe the response shown in figure 4. Unless stated otherwise the parameter values used are listed in table 1. It should be stated that these values are purely indicative rather than fit to any supplied physical dimensions and the valves were symmetric as derived in section 4.4. Nevertheless, the observed behaviour was found to be typical of that at other parameter values. The input displacement used is the nondimensionalised form of (41).

5.2.1 Compressibility

The effect of compressibility is to allow for a dependence upon the history of the motion. This produces hysteretic effects. The effect of changing the damping parameter β using (34) and (35) can be seen in figure 11. The values used

in this graph are the same as those used in [10] with the additional parameter ζ set to 1. The higher the value of β, the higher the hysteretic effect. The graph also illustrates the effect of having different coefficient values in compression and rebound. The coefficient values when in compression (negative velocity) are lower than for rebound, producing a shallower gradient on the force-velocity graph. Consequently, the relative effect of the compressibility of the fluid is reduced. In the limit, a high value of β will produce a force proportional to displacement alone. A very low β produces a force that is proportional to velocity as in section 2.

The effect of fluid compressibility can now be investigated using (39) and (40). The general effect of compressibility can be seen in figure 12 for $\beta = 1.9\text{x}10^{-9}$. The values in table 1 are for this value of β. This value was taken as it is typical of values used in [8][9][10]. The system shows many of the characteristics displayed in figure 4 with a delayed response to rapid changes in velocity and hystersis in plot (b). There are three main differences between the explicit model and the extended time-stepping model. The explicit model shown in figure 10 is much more responsive to changes in velocity. Figure 12 does not respond so quickly as displayed in the large negative force region. This is very similar to the required characteristics in figure 4. The second point to note is the introduction of hystersis into the force-velocity plot in direct contrast to plot (b) in figure 10. The gradients of the system are qualitatively the same indicating that compressibility does not affect the broad damping characteristics as the force is still proportional to velocity. Lastly the system now takes into account the dynamics of the spring. This can be seen in plot (a) of figure 12 as the trajectory passes the critical force around $G = \pm 2$. The influence of the spring valve is clearer in plot (b). Oscillations can be seen as the trajectory follows the blow-off gradient. The oscillations are clearer than for plot (a) as the velocity is increasing by a large amount in the blow-off region so extending the oscillations of the spring

The value taken for β is of great importance to the dynamics of the system. As suggested earlier in this section a value that is too large will produce a force that is largely proportional to displacement whereas an almost incompressible fluid will produce a force proportional to velocity similar to the explicit model. Figures 13 and 14 illustrates the case of high compressibility ($\beta = 10\text{x}10^{-9}$) and low compressibility ($\beta = 0.1\text{x}10^{-9}$) respectively. In the limiting case of a non-compressible fluid the force will be a function of input velocity alone as in section 2. In figure 14 there is little hystersis in the force-velocity graph (b). The valve is also open for most of the period as seen in the valve displacement vs time plot (d). The induced force oscillations are also more rapid in plot (b) and occur for a shorter time than in figure 12 for higher compressibility. The overall dynamics are very similar to figure 10, in particular the force against velocity plots. This is in direct contrast to the case of high compressibility in figure 13. The system now has a considerable amount of history dependence

introducing hysteresis into the force-velocity profile in plot (b). The system spends less time in the blow-off region since the valve remains closed inbetween the main force peaks. The influence of the dynamics of the spring valve is also reduced when compared to figures 12 and 14 and the general shape of the force vs time plot in plot (a) of figure 13 is approaching that of the input displacement in figure 9 as expected. It is useful to note that the maximum force, flows and spring displacements are all approximately the same for both high and low compressibility. The main difference between the two cases occurs in the low force region as the system remains here for longer if the compressibility is higher.

Figure 12 is clearly the better model when comparing the algbraic model to the time-stepping approach. It has been shown that the selection of β is important. The value used to produce table 1 and figure 12 uses a value within the limits set by Surace et al for hydraulic fluid used in automobile shock absorbers. The resulting force is qualitatively similar to the required profile suggesting the modelling technique is valid.

5.2.2 Orifice diameter

The physical properties will have a large influence over the dynamics of the system. Intuitively one of the most important factors will be the size of the main orifice in the piston. Figures 15 and 16 illustrate the case of the diameter of the orifice increased by 500% and reduced to 20% respectively. Changing the value of the orifice diameter, d, will change all of the dimensionless parameters in (39) and (40) so no direct link can be made to the calculations. The original system in (36) and (37) indicates that the orifice diameter affects the pressure loss due to the orifice (D_1 and D_2) only. This is useful to note when trying to understand the dynamics.

The orifice diameter dramatically affects the output force profile for the same input displacement. A larger orifice as in figure 15 has a shallower force-velocity gradient which produces vastly different dynamics since the valve is open for a shorter period of the cycle. This makes sense since the losses due to the orifice will be less so there will be less pressure to open the valve for a given piston velocity. There is also less hysteresis displayed in panel (b) although the oscillations due to the spring are still evident. While the compressibility means the system is not too responsive to changes in velocity, the forces generated for a large proportion of the motion are too small. This is again due to the reduced pressure difference from the orifice.

Decreasing the size of the orifice by a factor of 5 in figure 16 does not have such a large effect on the system when compared to the reference model in figure 12 since the dynamics are now dominated by the case when the valve

is open. Due to this the only noticable difference when decreasing the orifice diameter will be to reach the critical force sooner. In the case shown in figure 12 the critical force is reached quickly at which point the valve will open. While the valve is open the losses will be dominated by the flow past the valve as illustrated in plot (d). The pressure losses due to the orifice will remain approximately at the same level. By decreasing the size of the orifice there will be more flow past the valve. Since the force vs velocity profile is shallow for this blow-off section the effect on the force will be minimal.

5.2.3 Instability issues

As with many dynamical systems there are regions of parameter space that can cause the system to become unstable or cause the force to oscillate rapidly with a large amplitude. In the damper modelled the most likely module to become unstable is the spring valve system. Under certain conditions the spring can undergo high frequency oscillations as displayed in figure 17 where the spring damping has been reduced by a factor of $\frac{3}{5}$ from previously with a simple sinusoidal input of $1 \times 10^{-3} \sin(t)$. The rapid motion causes oscillations in the force generated as illustrated in (a). There are two time-scales exhibited for the given input profile: the large time period of the input motion; and the small time-scale spring oscillations.

There is a great deal of scope for investigation into these instabilities and when they occur. Factors such as the flow characteristics of the valve (values of γ and C_{po}) and the spring stiffness constant (k) cause similar oscillations. In extreme cases the numerical scheme cannot solve.

6 Optimisation

The aim of this section is to outline a method to test whether the current set up of the damper is optimal. To optimise a system there needs to be some basis to compare one set up from another. A typical controller for a damper system maximises the energy dissipation that results from the motion of the damper. If the modelled damper is taken the dimensions are set. This means the coefficients cannot be changed. The only degree of freedom available is the maximum allowable force. The effect of the spring dynamics are not considered here as it has no influence over the maximum force obtained. Similarly compressibility is also ignored for now.

The general equation for energy dissipation is given by force multiplied by displacement for a full cycle of operation,

$$\oint F dy \tag{42}$$

where F is the force and y is the displacement of the damper piston as before.

It is clear from (42) that the maximum energy would be dissipated if there was a large maximum force, or a large displacement. However, both of these are restricted. If there was a large resistive force from the damper there would be little motion from the piston so producing low dissipation. Conversely, if the piston was allowed to move freely there would be little resistance to motion (low force) and so low dissipation. This coupling of maximum force and maximum displacement suggests that there is an optimum value for each. As a first assumption, the relationship between maximum force (F_{max}) and maximum displacement (y_{max}) is given by

$$F_{max} = \frac{\xi}{y_{max}}, \tag{43}$$

where ξ is a constant taken as 1 for illustration.

The energy dissipated in (42) corresponds to 4 times the area under the force-displacement graph in figure 18. With a sinusoidal input however, analysis is simpler if calculated in the time domain. Equation (42) can be rewritten as

$$W_d = \int_0^{\frac{2\pi}{\omega}} F\left(\frac{dy}{dt}\right) dt$$

$$W_d = 4\int_0^{\frac{\pi}{2\omega}} F\dot{y} dt \tag{44}$$

for a symmetric set of equations (i.e. coefficients are the same for compression and rebound), where F is given by the linearised

$$F(t) = \begin{cases} d_1^{(1)}\dot{y} & \text{if } |F| < F_{crit}, \\ d_1^{(2)}\dot{y} + d_3^{(2)} & \text{if } |F| > F_{crit}, \end{cases} \tag{45}$$

where $d_3^{(2)}$ is calculated to give a smooth transition from low to high force, and

$$y = Y\sin(\omega t).$$

If the maximum velocity (V_{max}) can be calculated ($Y\omega$) then (45) can be solved for velocity using the point (V_{max}, F_{max}) as

$$F(t) = \begin{cases} d_1^{(1)}\dot{y} & \text{if } |F| < F_{crit}, \\ d_1^{(2)}\dot{y} + F_{max} - d_1^{(2)}V_{max} & \text{if } |F| > F_{crit}, \end{cases} \tag{46}$$

Equation (46) can then be used to find the intersection point as a function of F_{max} and V_{max} as the linearised system produces a straight line graph in the force-velocity plane. The time of intersection (t_{crit}) is then given as

$$t_{crit} = \frac{1}{w}\arccos\left(\frac{F_{max} - d_1^{(2)}V_{max}}{V_{max}(d_1^{(1)} - d_1^{(2)})}\right). \tag{47}$$

Using (43), (46) and (47), the integral in (44) can now be given as

$$\begin{aligned} W_d = 4\int_0^{\Psi}\left[\left(d_1^{(2)}Y\omega\cos(\omega t) + \frac{\xi}{Y} - d_1^{(2)}Y\omega\right)Y\omega\cos(\omega t)\right]dt \\ +4\int_{\Psi}^{\frac{\pi}{2\omega}}\left[d_1^{(1)}(Y\omega\cos(\omega t))^2\right]dt, \\ \text{where } \Psi = \frac{1}{w}\arccos\left(\frac{\frac{\xi}{Y} - d_1^{(2)}Y\omega}{Y\omega(d_1^{(1)} - d_1^{(2)})}\right). \end{aligned}$$

The equations are valid for

$$\frac{1}{\omega}\sqrt{\frac{\xi}{d_1^{(1)}}} < Y < \frac{1}{\omega}\sqrt{\frac{\xi}{d_1^{(2)}}}$$

as $0 < F_{crit} < F_{max}$.

With this information, a graph can be plotted for any set of parameters. An example is shown in figure 19. The optimal value for the maximum displacement is 1.228 m corresponding to 0.9550 Nm of energy dissipated. The critical force for this setup is calculated using

$$F_{crit} = Y\omega\cos(\omega t_{crit})$$

where t_{crit} is calculated in (47) giving F_{crit} a value of 0.72 N with F_{max} being 0.81 N from (43). F_{crit} is 89% of the maximum force.

The process above illustrates that an optimum critical force can be found. This corresponds to a stiffness of the relief valve spring. This could be used in the future if the spring valve was replaced by a semi-active servovalve.

7 Conclusion

The main result from this paper is that a damper with relief valve can be modelled with a parametrised system of equations. There are benefits and disadvantages associated with all the proposed models.

Section 2 summarised previous work on a simplified shock absorber. It is clear where the force is coming from and how the various parameters can affect the force profile. The model is also explicit and so requires negligable computation time for a given input. There are two main disadvantages however. The first is the unclear selection of $d_3^{(2)}$ in the blow-off region, hence the need for the models described by (9) and (10) without the valves and (20), (21) and (22) with the valve. The second reason for not using the model is the rapid response to changes in input velocity. The model does not incorporate any hysteresis or delay for rapid changes in velocity. Tests suggest that there is a need for some kind of delay as in (34) and (35).

There are two approaches to address the issue of the transition from low to high forces: modelling the system without a dynamic relief valve as in (9) and (10); or including the relief valve as a system state with (20), (21) and (22). The first approach assumes that the relief valve is either open or closed and makes modelling assumptions to get from the valve always closed to always open. While this approach gives qualitatively more realistic results, there is no formal justification for the valve assumption. The second method incorporates the additional head loss due to the relief valve. The flow is then shared in some proportion between the valve and the main orifice. Again this gives good results and has the benefit of a physically justifiable basis. However as with (7), a major problem with both models is the lack of delay.

Incorporating the compressibility effects of the hydraulic fluid produces (34) and (35). This approach leads to a delay in the system's response to changes in velocity. Equations (39) and (40) combine all of the new effects introduced into a single nondimensional model. The basic compressibility model is used with the full relief valve model. This system gives qualitatively correct results for the whole working cycle. The only disadvantages are the complexity of the model and the fact that it must now be solved by time-stepping. For the purpose of this report a 4th order Runge-Kutte scheme was implemented which yielded repeatable results. The final combined model is clearly the best option as it incorporates all the required dynamics of the system including the motion of the spring valve and a form of hysteresis. We believe we now have a parametric model that is fully able to capture these results (see figure 12) and more importantly enables the designer to consider optimisation and parameter studies. The sketch in figure 4 displays the main characteristics of the damper to be modelled in this paper. This is based on test results which

were not conducted by the authors and for which no quantitative results were available.

The final model can be used in three situations:

i simulating the resulting force from a given displacement input;
ii simulating the motion of the piston from a given force input; and
iii simulating the damper as part of a large coupled system with force linked to displacement.

This paper focused on the first case. The parameters calculated for this situation can be used to calibrate the model for the other two uses. The effect the complex motion of the damper may have on the entire system dynamics will be taken up in future work.

In section 6 the possible optimisation of the damper system to increase the energy dissipated was considered. The process made simplifying assumptions about the input profile and the effects of the spring valve and compressibility. Nevertheless, the technique employed produced a solution that can be used to compare configurations. The parameters used have direct links to the dimensions and properties of the damper to allow immediate changes to the system.

There are several factors that have not been taken into account when producing the model. These include:

i backlash (not used but discussed in (12));
ii the compressibility of the damper casing, discussed in [8];
iii impact dynamics of the spring valve on the valve seat;
iv the issue of cavitation between high and low pressure regions (formation of bubbles); and
v the dependence of viscosity on temperature.

Backlash would be the easiest to model as in section 4.1. The other factors are not so straightforward and are problems to be addressed in future work. The temperature issue will arguably give the largest effect when trying to produce an accurate model. The oil used in a typical hydraulic component is MIL-H-5606 standard hydraulic fluid. An approximate relationship for the change in viscosity over a range of temperatures can be seen in (48) from reference [21], where η is the viscosity and T is the absolute temperature. A, B and S are constants to be determined. By curve-fitting using data from Fisher Regulators, S = 1270, A = 5×10^{12} and B = 16.5.

$$\eta = A\left(\frac{T}{S}\right)^{\frac{T}{B}} \tag{48}$$

Example values are η=16cP for 38^{o}C and η=5.7cP for 93^{o}C. This is a large difference which should not be ignored as the dynamics of (7) are strongly dependent upon the viscosity. A higher temperature implies a lower force-velocity gradient as the fluid is less viscous. Clearly such effects are likely to have significe the start up of mechanical devices such as in automotive and aerospace applications, where the characteristics of the damper are likely to be widely different than at the final operating temperature.

References

[1] J. Wallaschek, Dynamics of non-linear automobile shock absorbers. International Journal of Non-Linear Mechanics 25(2/3) (1990) pp.299-308.

[2] W.N. Patten, R.L. Sack, Q. He, Controlled semi-active hydraulic absorber for bridges. Journal of Structural Engineering 122(2) (1996) pp.187-192.

[3] B. Panda, E. Mychalowycz, F.J. Tarzanin, Application of passive dampers to modern helicopters. Smart Materials and Structures 5 (1996) pp.590-516.

[4] G.M. Kamath and N.M. Wereley and M.R. Jolly, Characterisation of magnetorheological helicopter lag dampers. Journal of the American Helicopter Society July (1999).

[5] S. Marathe and F. Gandhi and K.W. Wang, Helicopter blade response and aeromechanical stability with a magnetorheological fluid based lag damper. Journal of Intelligent Material Systems and Structures 9 (1998) pp.272-282.

[6] A.A. Seleemah, M.C. Constantinou, Investigation of seismic response of buildings with linear and nonlinear fluid viscous dampers. National Centre for Earthquake Engineering Research NCEER-97-0004 (1997).

[7] G.W. Housner, L.A. Bergman, T.K. Caughey, A.G. Chassiakos, R.O. Claus, S.F. Masri, R.E. Skelton, T.T. Soong, B.F. Spencer, J.T.P. Yau, Structural engineering: past, present and future. Journal of Engineering Mechanics 123(9) (1997) pp.897-971.

[8] C. Surace, K. Worden, G.R. Tomlinson, An improved nonlinear model for an automotive shock absorber. Nonlinear Dynamics 3 (1992) pp.413-429.

[9] C. Surace, K. Worden, G.R. Tomlinson, On the nonlinear characteristics of automotive shock absorbers. Proceedings of the Intsitute of Mechanical Engineers Part D: Journal of Automobile Engineering 206(1) (1992) pp.1-16.

[10] S. Cafferty, K. Worden, G.R. Tomlinson, Characterization of automotive shock absorbers using random excitation. Proceedings of the Intsitute of Mechanical Engineers Part D: Journal of Automobile Engineering 209(4) (1995) 239-248.

[11] C. Surace, D. Storer, G.R. Tomlinson, Characterising an automotive shock absorber and the dependance on temperature. Proceedings of the 10^{th} International Modal Conference (1991) pp.1317-1326.

[12] M.A. Dokainish, M.M. Elmadany, On the non-linear response of a relief valve. ASME Journal of Mechanical Design 100 (1978) pp.675-680.

[13] A.H. Nayfeh, H. Bouguerra, Non-linear response of a fluid valve. International Journal of Non-Linear Mechanics 25(4) (1990) pp.433-449.

[14] S. Hayashi, T. Hayase, T. Kurahashi, Chaos in a hydraulic control valve. Journal of Fluids and Structures 11(6) (1997) pp.693-716.

[15] H.H. Lang, A Study of the characteristics of automotive hydraulic dampers at high stroking frequencies, PhD Thesis, Department of Mechanical Engineering University of Michigan, 1997.

[16] H.A. Barnes and J.F. Hutton and K. Walters, An Introduction to Rheology, Elsevier, 1989.

[17] J.A. Roberson, C.T. Crowe, Engineering Fluid Mechanics (Sixth Edition), John Wiley and Sons, Inc. 1997.

[18] R.W. Jeppson, Analysis of Flow in Pipe Networks, Ann Arbor Science, Michigan, 1976.

[19] T.T. Soong, M.C. Constantinou, Passive and active structural vibration control in civil engineering, Springer, 1994.

[20] The MathWorks Inc, MATLAB version 6.1, 2001.

[21] A Hussain, S. Biswas, K. Athre, A new viscosity-temperature relationship for liquid lubricants. WEAR 156 (1992) pp.1-18.

Fig 1: A simplified model of a damper.
Fig 2: Blow-off valve in damper.
Fig 3: A sketch of a typical input displacement against time.
Fig 4: A sketch of the required force output against time and velocity.
Fig 5: Analogous model of damper.
Fig 6: Simplified equivilent head loss for (9). Note the construction of the fictitious constant $d_3^{(2)}$.
Fig 7: Effect of including inertia of piston. Magnified region at maximum acceleration.
Fig 8: Effect of changing parameter values in (8). Unless stated $d_1^{(1)} = 1$, $d_2^{(1)} = 1$, $d_1^{(2)} = 0.2$, $d_2^{(2)} = 0$, $F_{crit} = 0.5$. $-.-$ $d_2^{(1)} = 0$, $-+-$ $F_{crit} = 0.2$, $-\diamond-$ $d_1^{(1)} = 2$.
Fig 9: Example input displacement using (41). Nondimensionalised as in section 4.4.
Fig 10: Applying algebraic equation to input in (41). (a) Force against time, (b) Force against velocity. $d_1^{(1)} = 5\times10^4$, $d_2^{(1)} = 1\times10^3$, $d_1^{(2)} = 5\times10^3$, $d_2^{(2)} = 0$, and $f_{crit} = 2\times10^6$.
Fig 11: Effect of changing the compressibility of the fluid in the damper with sinusoidal displacement input.
Fig 12: $\beta = 1.9\times10^{-9}$. (a) Force against time for 2 periods; (b) Force against velocity; (c) Dynamics of the valve; and (d) Difference in flow between orifice and valve.
Fig 13: $\beta = 10\times10^{-9}$. (a) Force against time for 2 periods; (b) Force against velocity; (c) Dynamics of the valve; and (d) Difference in flow between orifice and valve.
Fig 14: $\beta = 0.1\times10^{-9}$. (a) Force against time for 2 periods; (b) Force against velocity; (c) Dynamics of the valve; and (d) Difference in flow between orifice and valve.
Fig 15: d is 500% larger. (a) Force against time for 2 periods; (b) Force against velocity; (c) Dynamics of the valve; and (d) Difference in flow between orifice and valve.
Fig 16: d is 20% of original. (a) Force against time for 2 periods; (b) Force against velocity; (c) Dynamics of the valve; and (d) Difference in flow between orifice and valve.
Fig 17: High amplitude oscillations of spring with sinusoidal input. Spring damping, δ, 60% less than used for table 1. (a) Force against time; (b) Force against velocity; (c) Dynamics of the valve; and (d) Difference in flow between orifice and valve.
Fig 18: Force vs displacement for a quarter cycle with blow-off at (y_{crit}, F_{crit}).
Fig 19: Work done against stroke length for ξ=1, $d_1^{(1)}$=2, $d_2^{(1)}$=0.1, ω=1.

Parameter	Value	Units
ξ	$1.39\text{x}10^{6}$	N/m^2
f	$5.55\text{x}10^{3}$	N
T	0.033	s
ν	$1.3\text{x}10^{-4}$	m
h	11.9	m
Z_{crit}	1.8	-
c_1	$1.65\text{x}10^{3}$	-
c_2	$2.18\text{x}10^{4}$	-
c_3	1.8	-
c_4	$9.03\text{x}10^{12}$	-
c_5	$4.75\text{x}10^{6}$	-

Table 1: Parameter values used in sections 5.1 and 5.2

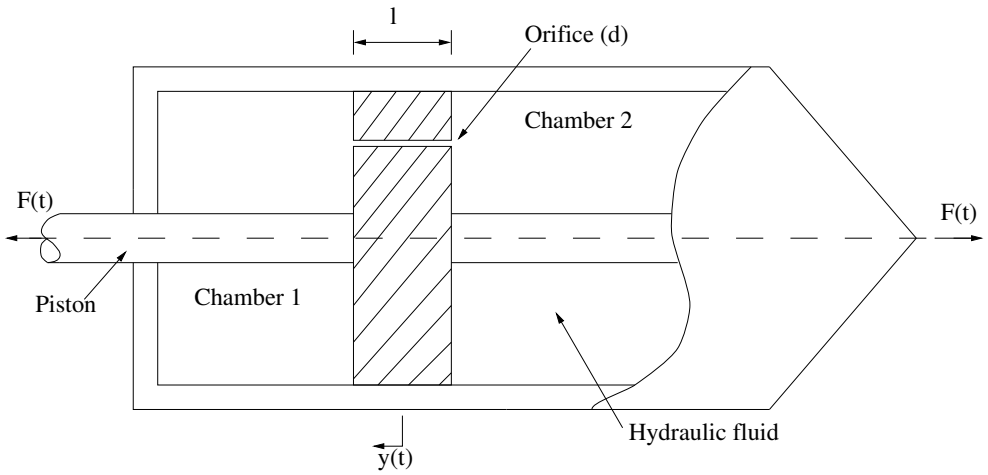
l
Orifice (d)
Chamber 2
F(t)
F(t)
Piston
Chamber 1
Hydraulic fluid
y(t)

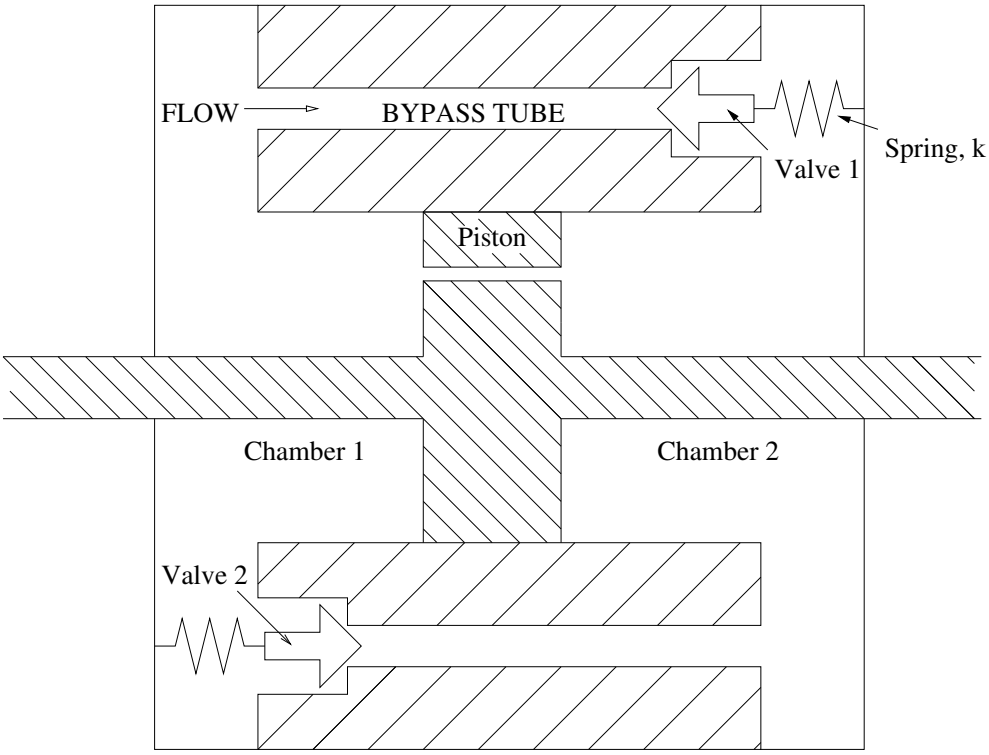
FLOW
BYPASS TUBE
Valve 1
Spring, k
Piston
Chamber 1
Chamber 2
Valve 2

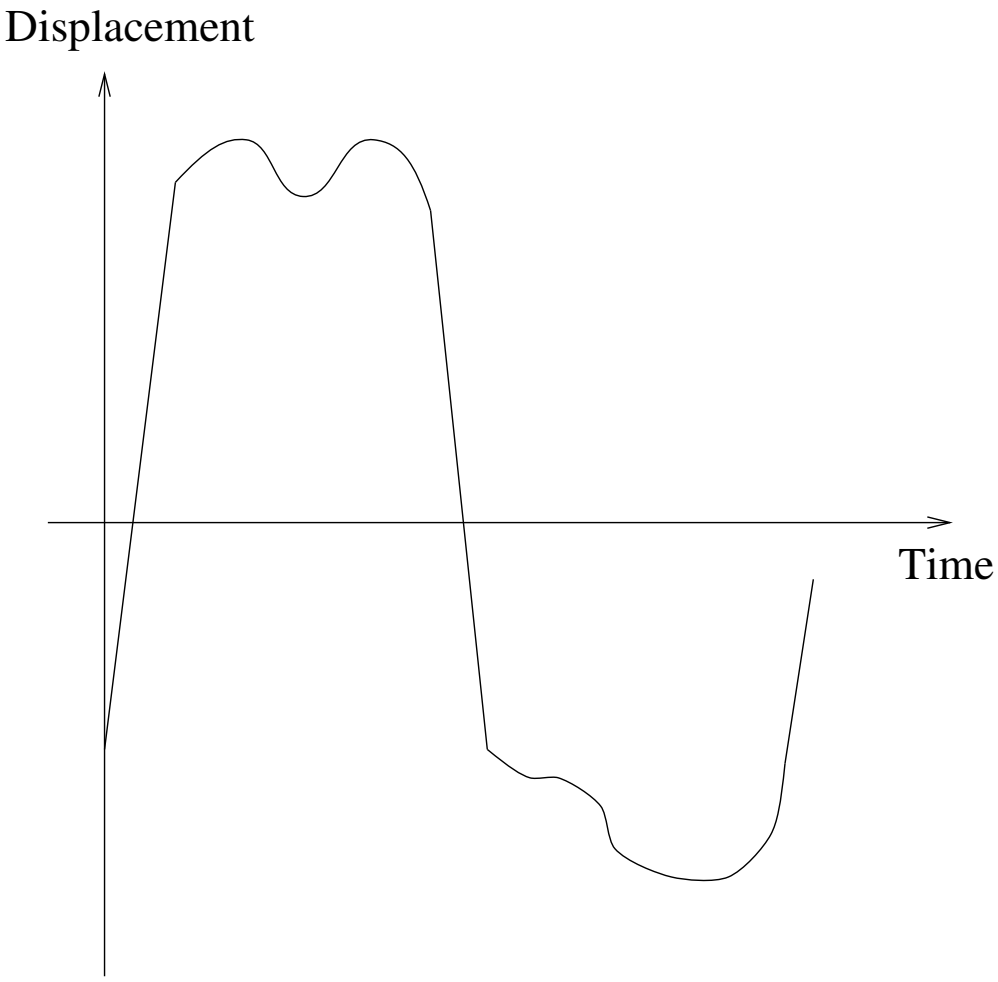
Displacement
Time

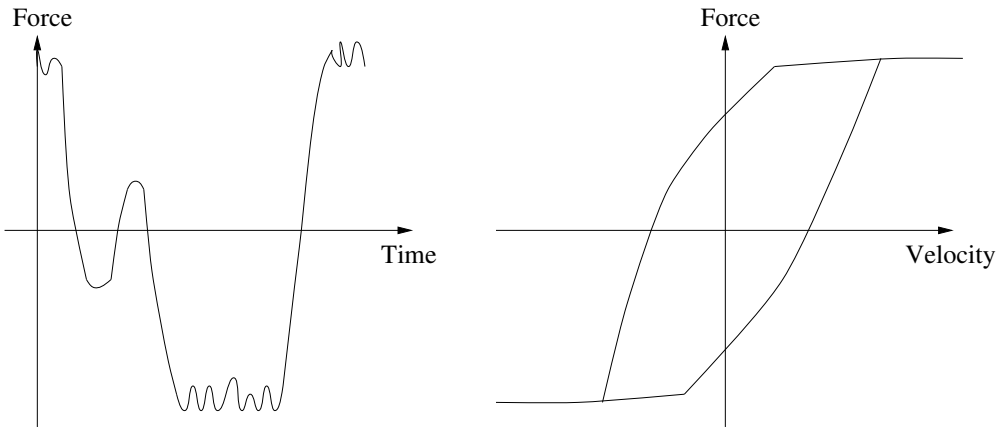
Force
Time
Force
Velocity

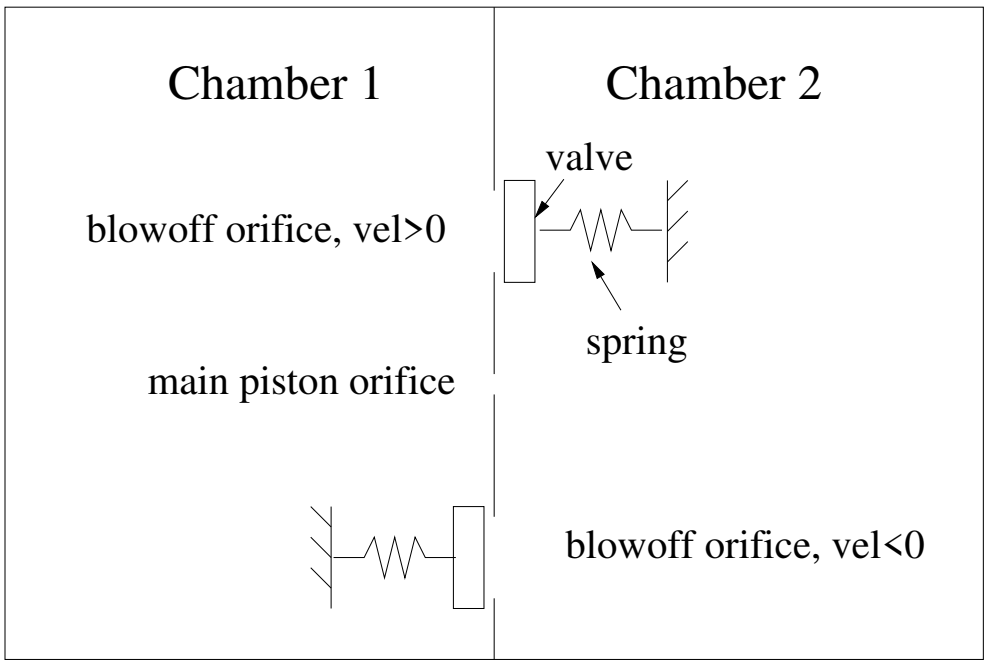
Chamber 1
Chamber 2
valve
blowoff orifice, vel>0
spring
main piston orifice
blowoff orifice, vel<0

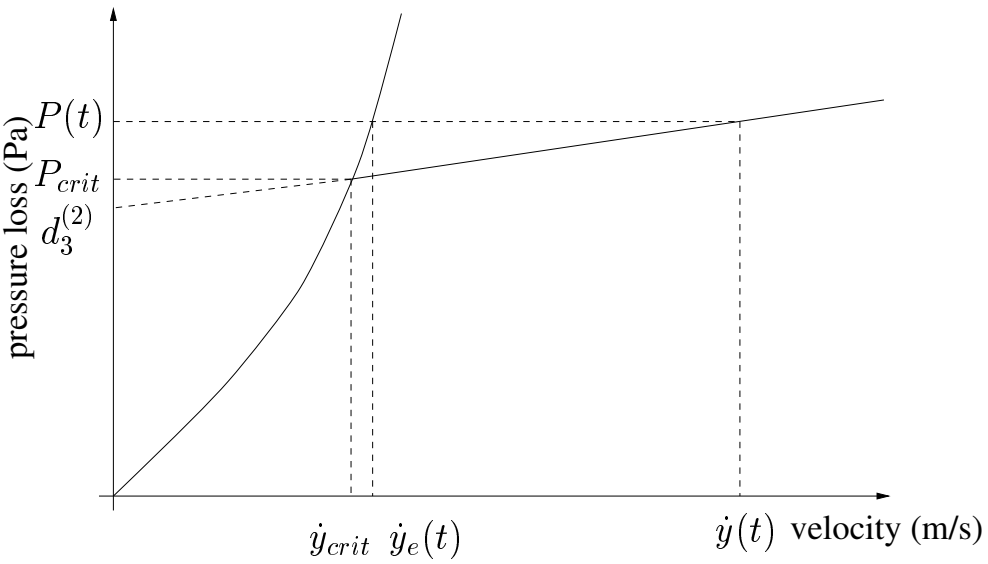
pressure loss (Pa)
$P(t)$
P_{crit}
$d_3^{(2)}$
$\dot{y}_{crit}$
$\dot{y}_e(t)$
$\dot{y}(t)$
velocity (m/s)

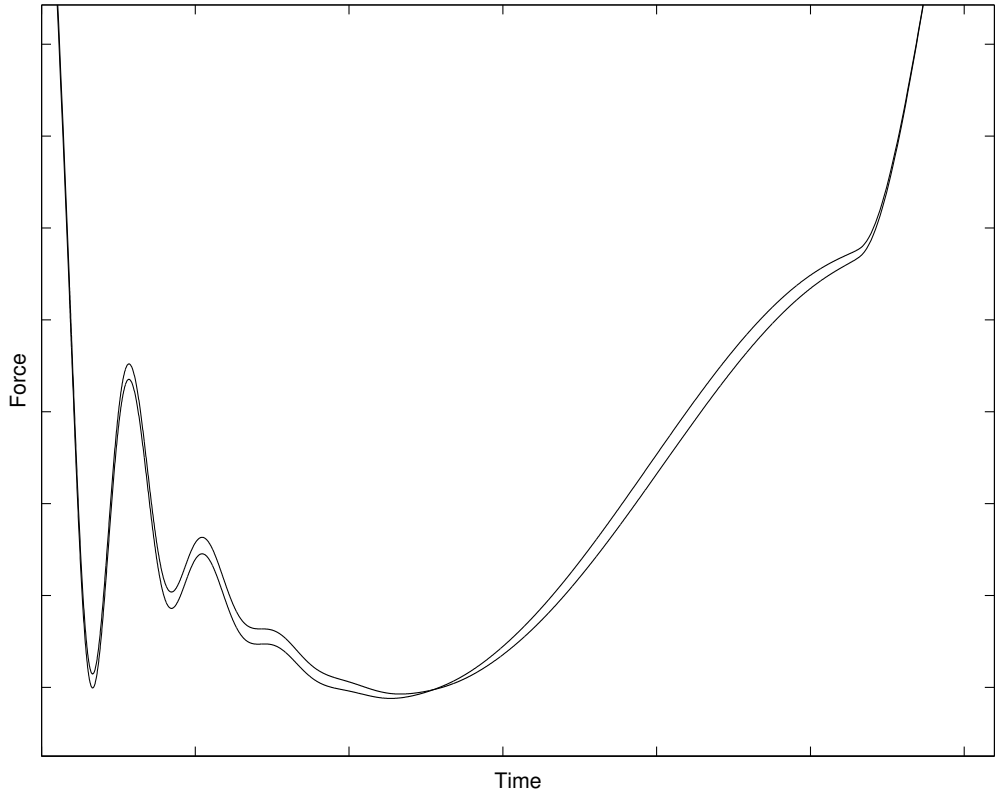
Force
Time

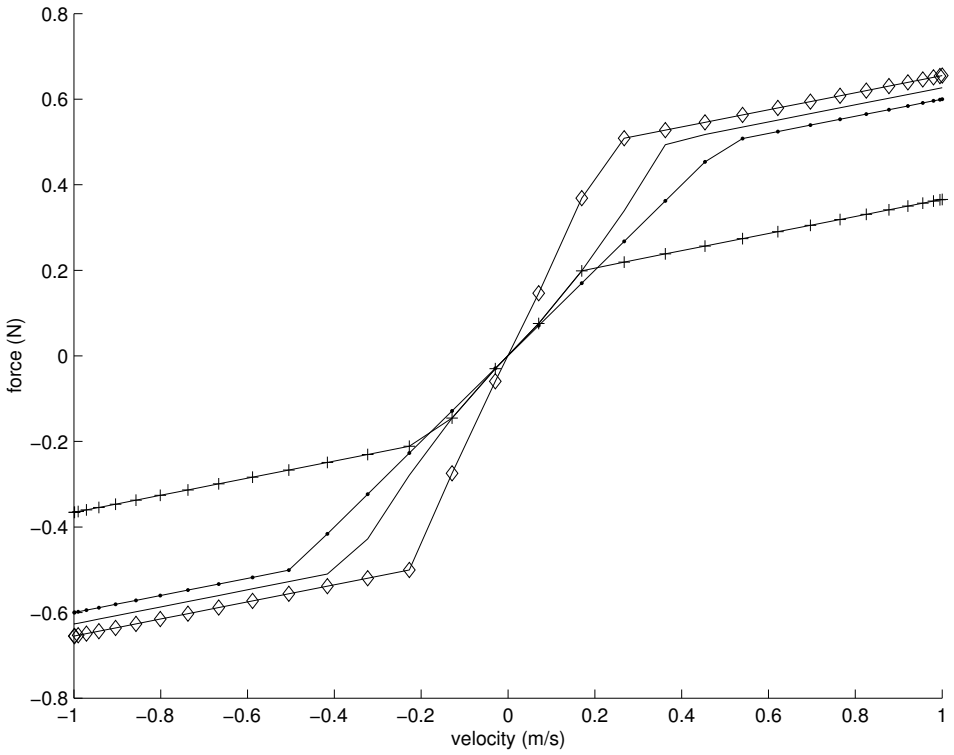
0.8
0.6
0.4
0.2
0
−0.2
−0.4
−0.6
−0.8
force (N)
−1
−0.8
−0.6
−0.4
−0.2
0
0.2
0.4
0.6
0.8
1
velocity (m/s)

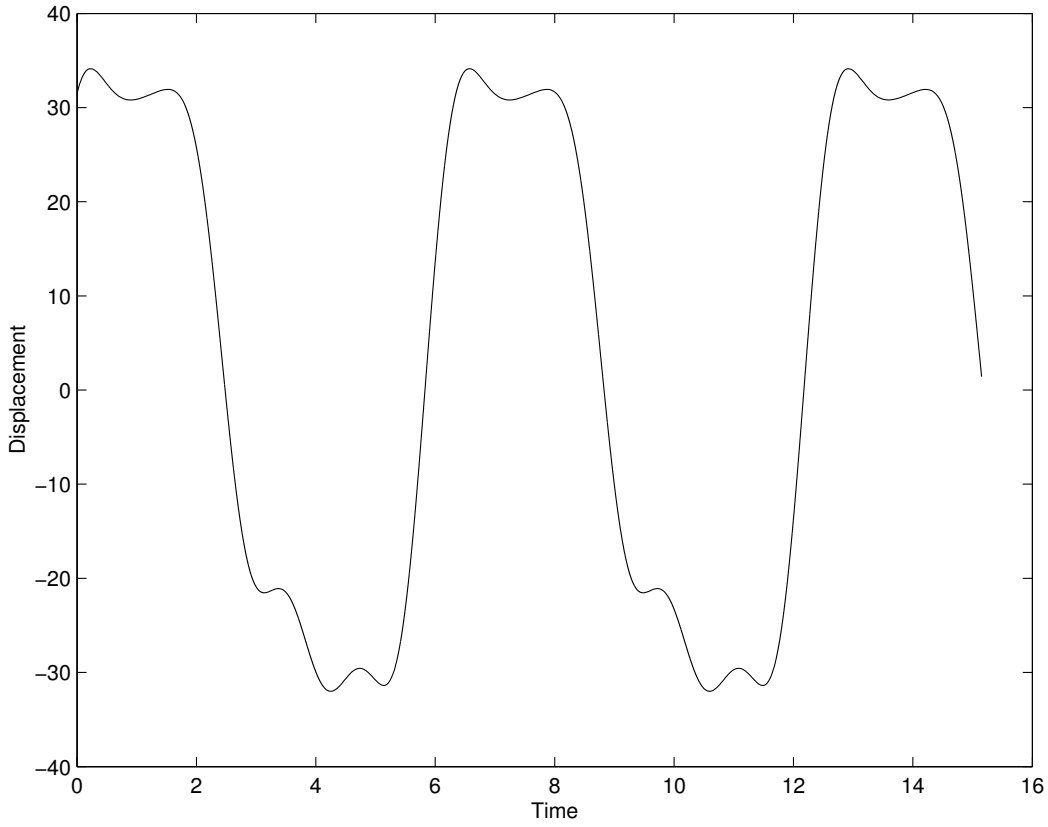
Displacement
Time
40
30
20
10
0
−10
−20
−30
−40
0
2
4
6
8
10
12
14
16

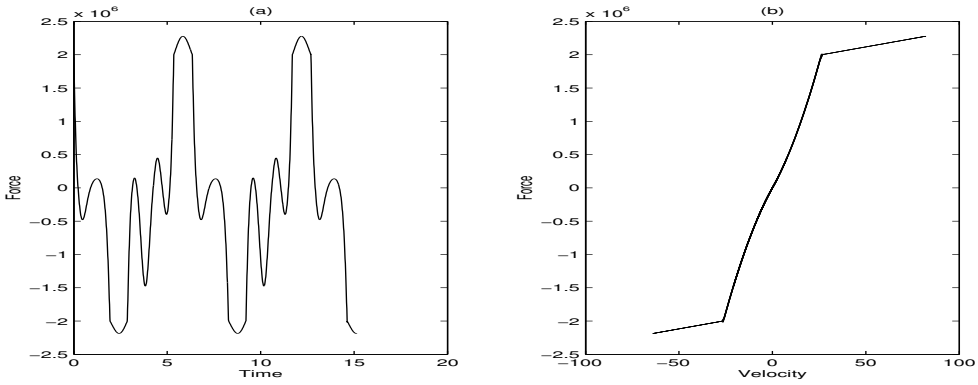
(a)
x 10^6
Force
Time
(b)
x 10^6
Force
Velocity

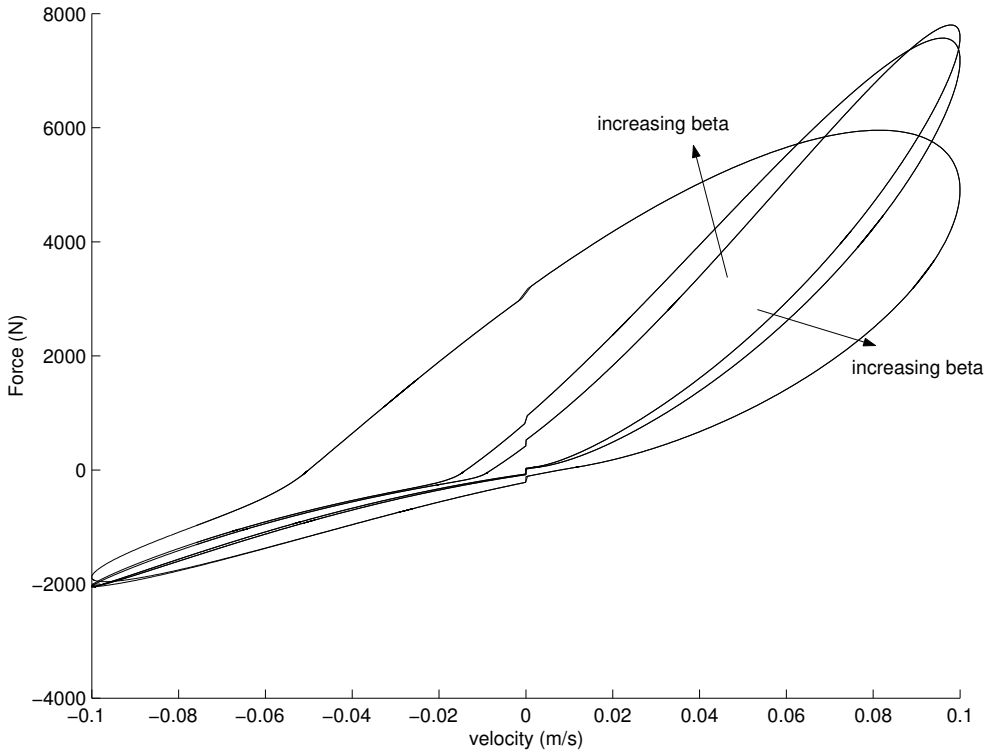
8000
6000
4000
2000
0
−2000
−4000
Force (N)
−0.1
−0.08
−0.06
−0.04
−0.02
0
0.02
0.04
0.06
0.08
0.1
velocity (m/s)
increasing beta
increasing beta

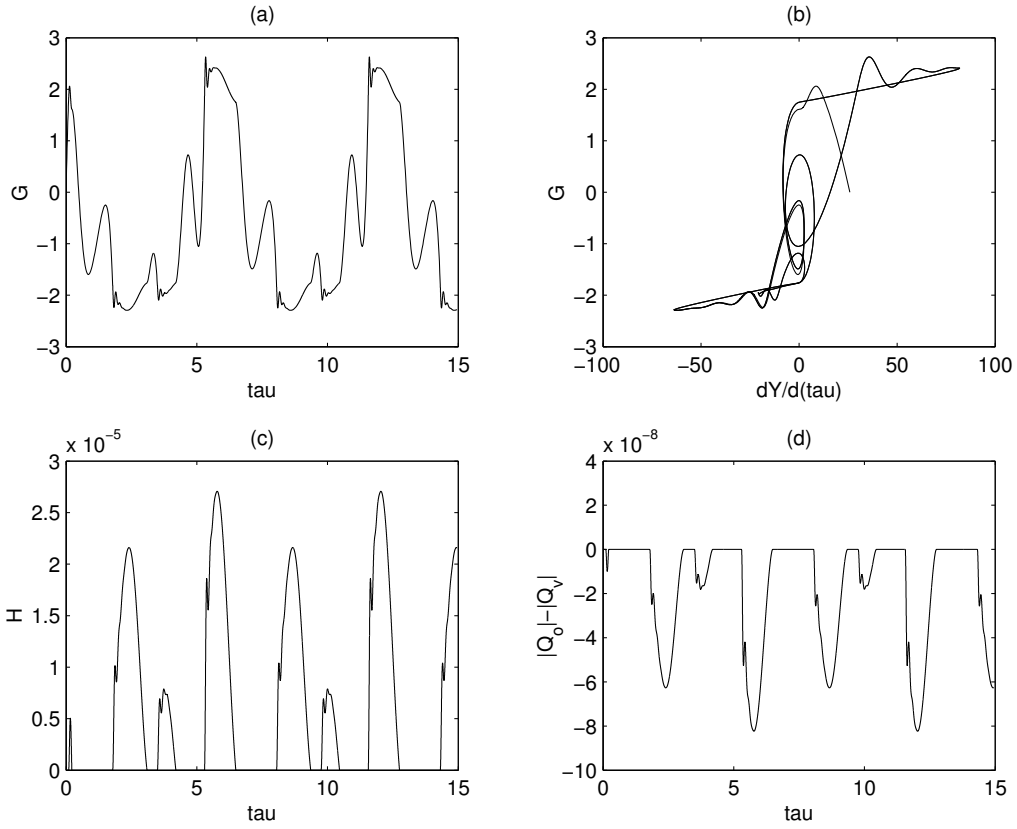
(a)
G
tau
(b)
G
dY/d(tau)
(c)
x 10^-5
H
tau
(d)
x 10^-8
|Q_o|−|Q_v|
tau

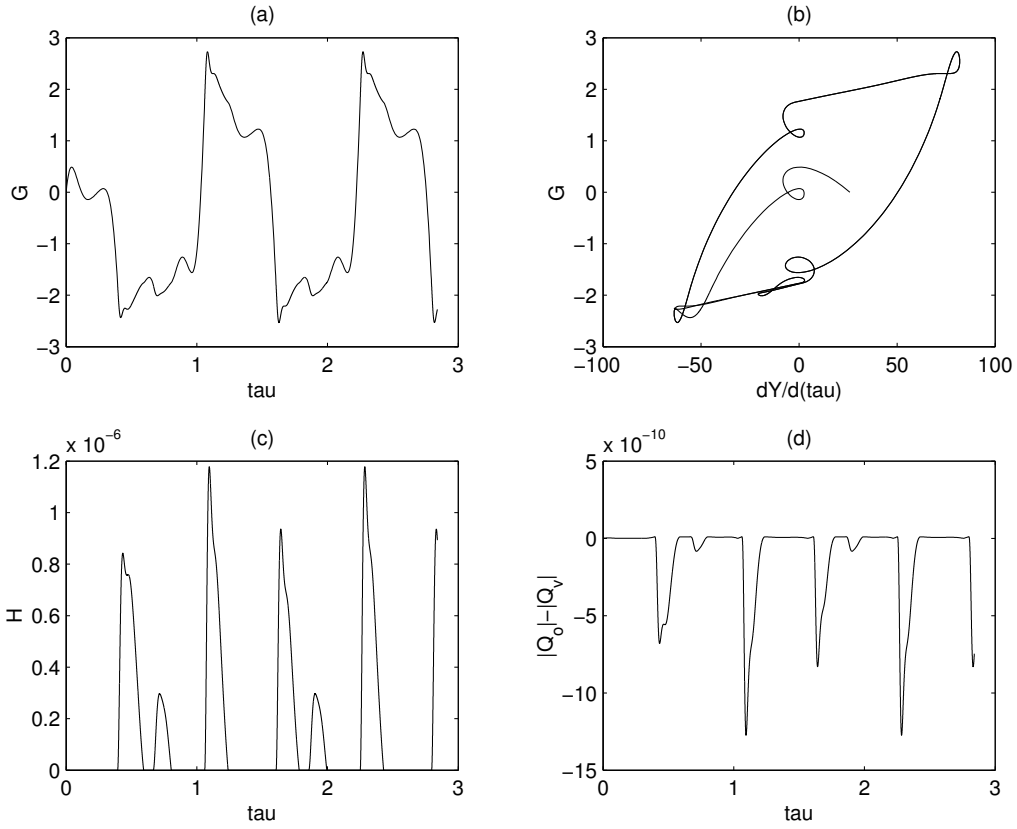
(a)
G
tau
(b)
G
dY/d(tau)
(c)
x 10^−6
H
tau
(d)
x 10^−10
|Q_o|−|Q_v|
tau

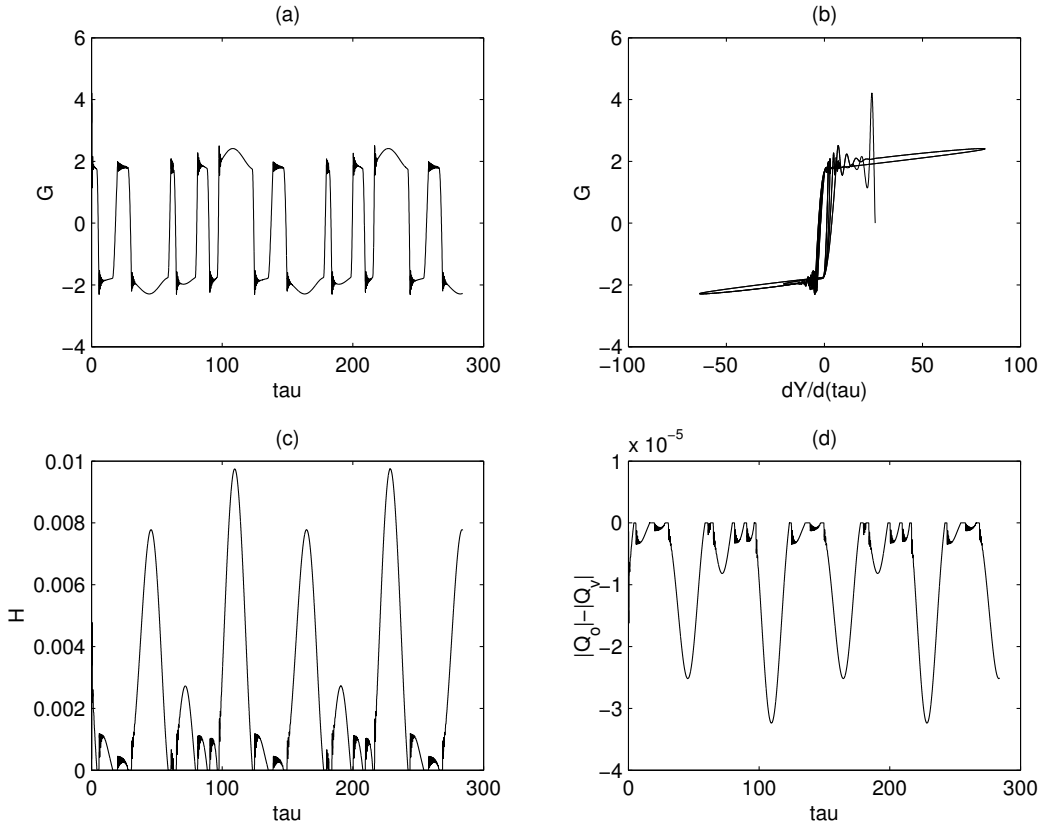
(a)
G
tau
(b)
G
dY/d(tau)
(c)
H
tau
(d)
x 10^-5
|Q_o|−|Q_v|
tau

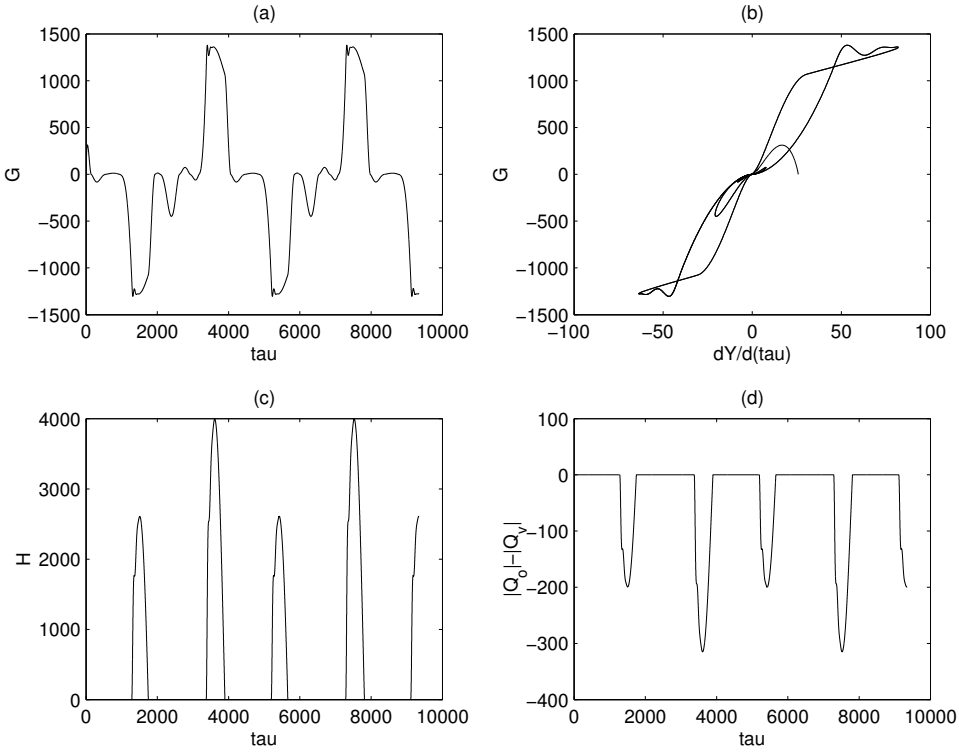
(a)
G
tau
(b)
G
dY/d(tau)
(c)
H
tau
(d)
|Q_o|−|Q_v|
tau

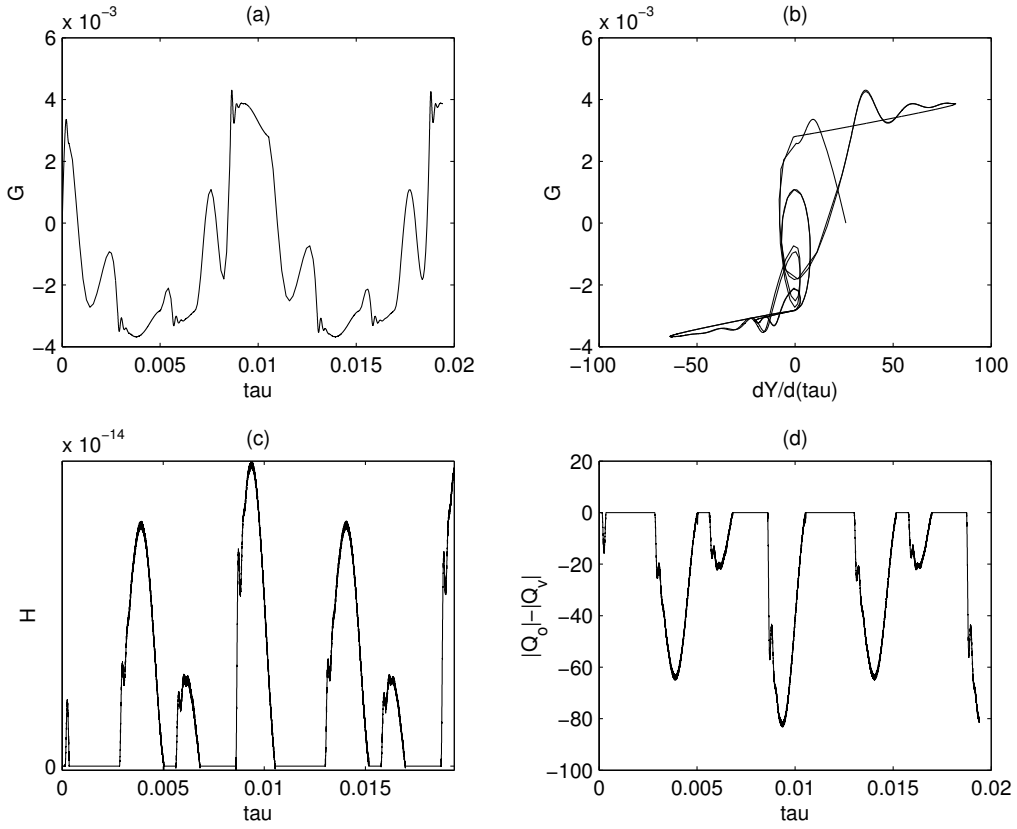
(a)
x 10^-3
G
tau
(b)
x 10^-3
G
dY/d(tau)
(c)
x 10^-14
H
tau
(d)
|Q_o|−|Q_v|
tau

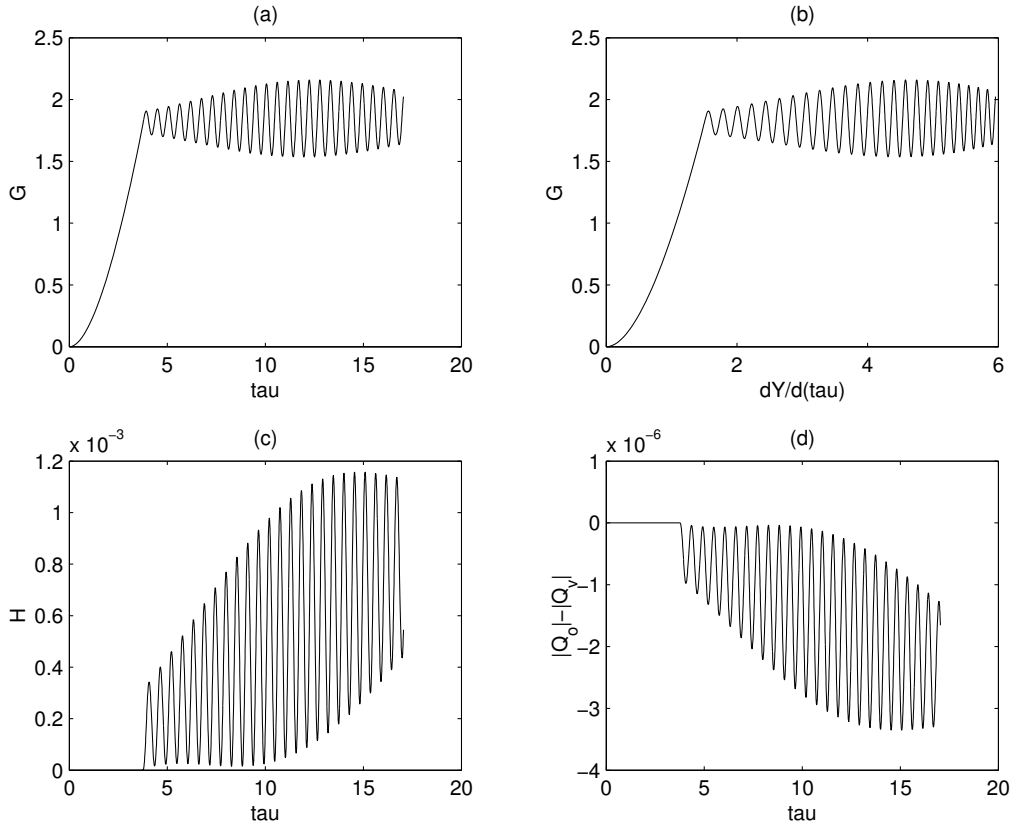
(a)
G
tau
(b)
G
dY/d(tau)
(c)
x 10^−3
H
tau
(d)
x 10^−6
|Q_o|−|Q_v|
tau

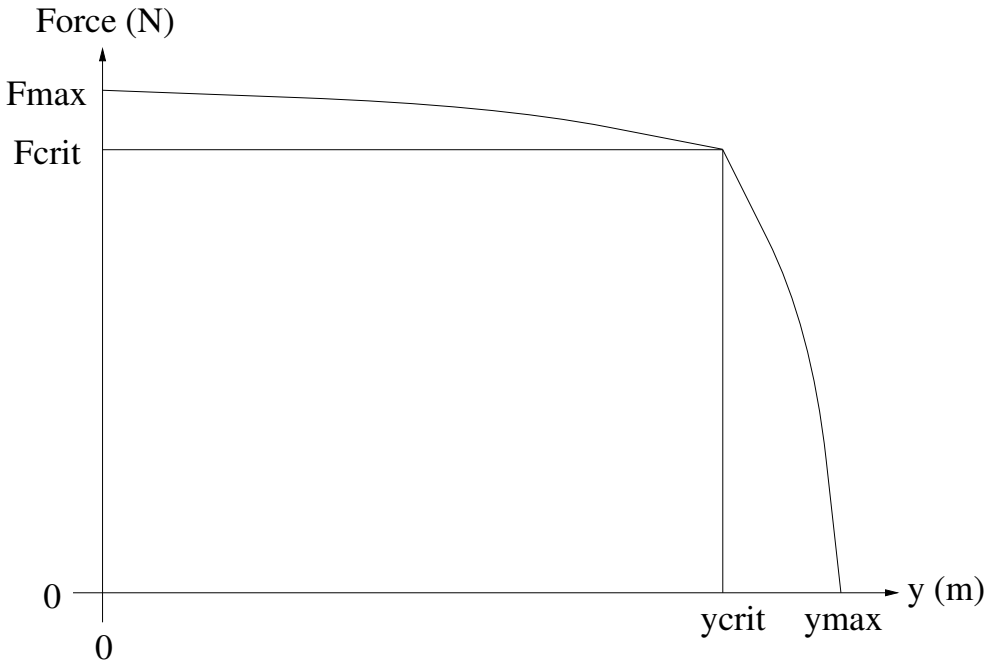
Force (N)
Fmax
Fcrit
0
0
ycrit
ymax
y (m)

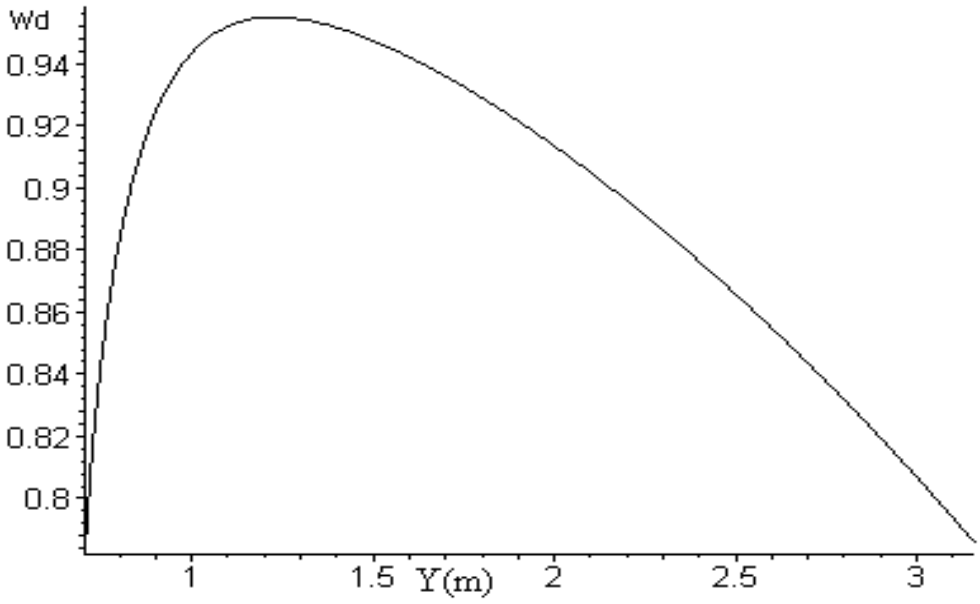
Wd
0.94
0.92
0.9
0.88
0.86
0.84
0.82
0.8
1
1.5
Y(m)
2
2.5
3